Chapter 3

The growth and characterisation of $CuGaSe_2$ films

Various deposition techniques have been reported[116] for the growth of chalcopyrite compounds, which include physical evaporation of the elements (PVD), molecular beam epitaxy (MBE), selenisation/sulfurisation of metal precursors or rapid thermal processing (RTP), electrodepositon and chemical vapour deposition (CVD). As the material quality strongly depends on the deposition conditions and the substrate conditioning[117, 118], it is of general interest to develop approaches for the growth of the base materials of thin-film solar cells on large area substrates, targeting low production costs while maintaining satisfactory PV figures. Recently, physical evaporation methods have been introduced in industrial production of solar modules[119]. Nonetheless, it is accepted that moderate temperatures constitute a major requirement for industrial up-scaling of solar cell production, as the energy consumption during processing will be included in the final €/kWh ratio of the final product.

Growth methods based on chemical vapour deposition constitute an interesting approach, as they relax the requirements of high processing temperatures and high-vacuum conditions characteristic of evaporation-based processes. In this chapter, the main features of the open-tube chemical vapour deposition (CVD) system employed in this work for the growth of polycrystalline $CuGaSe_2$ (CGSe) thin films for PV applications will be reviewed, highlighting those aspects of film characterisation directly related to the subsequent processing of solar cells based on these films. In particular, the appearance of secondary phases as a function of the system operating conditions will deserve some attention in Section 3.3. Finally, it will be shown in Section 3.4 that the operation flexibility that characterises the open-tube CVD system allows the introduction of sequential deposition processes, as well as the use of metal precursors, for the growth of CGSe thin films. These approaches, well established in other technologies of film growth, constitute alternative methods able to overcome those difficulties found in the growth of films from single stage processes that will be reviewed in the following.

3.1 The open-tube CVD system

The open-tube CVD concept was designed as a convenient intermediate way between high-temperature and vacuum-based deposition processes (e.g. PVD, MBE) on the one hand, and processes characterised by long deposition times, despite of a high-quality material yield (e.g. closed-tube CVD, MOCVD) on the other hand, for the growth of polycrystalline thin-films of CGSe. The fundamental design concept lies on the chemical transport of species from a material source to the deposition area induced by a temperature gradient set up between these two sites.

CVD is a common technique for the growth of crystalline I-III-VI_2 materials in evacuated and sealed ampoules, where fixed amounts of raw material and transport species, normally halogens, are introduced in advance. The temperature gradient set in the reactor modifies the saturation conditions of the gaseous species along the ampoule, favouring volatilisation reactions on the source side between the load and the highly reactive transport species via the formation of halide species, and condensation reactions into the solid phase on the substrate side. The transport species is recycled, acting as a catalyst, and following closed loops from the source to the substrate side and back, until the process is stopped. The main advantages of CVD-based deposition processes are the significant reduction of required source temperatures, due to the active role of the halogen species in volatising metallic elements, compared to co-evaporation techniques, and the high crystalline quality and large crystal size achieved in the final samples.

In the open-tube CVD approach to the growth of polycrystalline films, a continuous gas flow sweeps the quartz reactor from the source side to the substrate side. The temperature gradient controls the transport of species, whereas the source and substrate temperatures determine respectively the volatilisation and deposition rates, together with the amount of transport gas offered to the load. Contrarily to the case of closed systems, the flux of transport gases can be externally controlled during the deposition process, providing a large flexibility in adjusting the final film composition of the samples.

CGSe films were grown in the frame of this work in an open-tube CVD system designed in cooperation between the Hahn-Meitner-Institut Berlin and the company Aixtron[120], on the basis of a modified commercially available III-V epitaxy set-up. Details of the set up and the CVD principle, as well as on preliminary structural characterisation of single-stage grown CGSe films, can be found in previous works[121, 79]. In the following, those aspects of the film growth which were found to have a direct influence on the subsequent processing of solar cells are presented.

A scheme of the open-tube CVD set up is depicted in Figure 23. Its main features are summarised in the following points:

- The reactor consists of an open quartz tube with a five-zone heater system along it. A turbo-pump unit and a pressure controller (not shown in the figure) at the gas outlet on the right side regulate the pressure in the reactor, kept at 100 mbar under working conditions. The temperature of each zone heater can be changed independently, allowing to set different temperature gradients between the source and substrate side. In standard processing (see Appendix I), the source temperature is set at 600°C, while the substrate temperature lies in the range 450-550°C. These temperatures are controlled by means of thermocouples situated directly beneath the source boats and the sample holder, respectively.
- Two sources are used as load, namely, Cu_2Se and Ga_2Se_3, which are synthesised from the elements prior to their use in the CVD reactor. The use of independent binary sources ensures the stoichiometric volatilisation of species[122] and provides a larger flexibility in the preparation of films with various compositions.
- Independent provision of halogen species iodine and chlorine are supplied respectively to the Cu_2Se and Ga_2Se_3 source boats, using H_2 as carrier gas.

Chlorine is provided as gaseous HCl from a pressurised bottle, whereas iodine is volatilised in an independent oven under H_2 at typical temperatures between 40 and 70°C.

- Incoming gas flows are controlled by mass flow controllers (denoted with Q in the figure). The HCl flux Q_{HCl} (typically 160 ml/min) is diluted in H_2 (Q_4 =300 ml/min), whereas the I_2/HI mixture is controlled by the injected H_2 flow Q_1 through the iodine source and a pressure controller at the outlet. The iodine oven temperature T_{Iodine} and the gas flow through the iodine source determine the flux of the reactive gaseous mixture I_2/HI sweeping the Cu_2Se boat. This flux is further diluted in H_2, controlled by Q_2 (typically Q_1+Q_2=460 ml/min). The I_2/HI line is kept at T>T_{Iodine} until the reactor entrance with an independent heating system, in order to avoid iodine deposition in the line. A purge-source H_2 flux Q_3 (~1000 ml/min) acting as carrier gas avoids back-diffusion of the gaseous species, driving the gas mixture towards the substrate side.
- The substrates are placed on a rotating sample holder, driven by an additional carrier-gas line, to improve the film homogeneity. The rotation velocity can be adjusted by a mass flow controller (not shown in the figure). Samples up to 5x5 cm^2 area can be used as substrates.

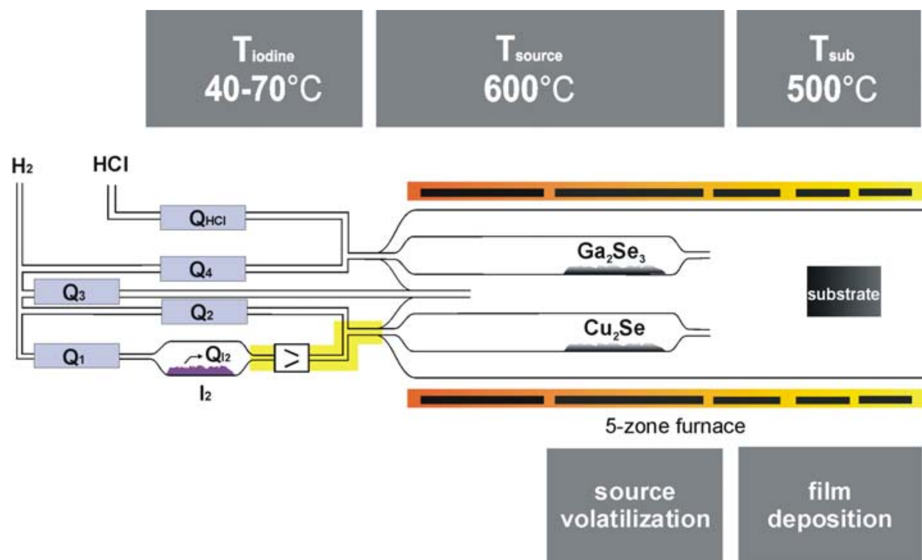

Figure 23. Schematic overview of the open-tube CVD system under working conditions (after[79]). Q-boxes in the incoming lines denote mass flow controllers. A pressure controller regulates the outlet of the iodine source. The I_2/HI line is maintained at T>T_{Iodine}.

Thermodynamic equilibrium calculations simulating the CVD process helped stating the dominant chemical reactions on the source side under typical working conditions (T_{source}= 600°C, p =100 mbar), according to the equations[123]:

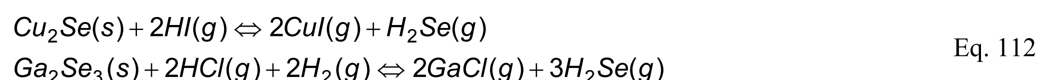

$$Cu_2Se(s) + 2HI(g) \Leftrightarrow 2CuI(g) + H_2Se(g)$$
$$Ga_2Se_3(s) + 2HCl(g) + 2H_2(g) \Leftrightarrow 2GaCl(g) + 3H_2Se(g)$$

Eq. 112

These equilibrium reactions predict the formation of gaseous halide species for the cation transport. Se transport is realised in the form of H_2Se. Additionally, it is also inferred from Eq. 112 that the Se provision is largely controlled by the Ga_2Se_3 line. We will come back to this point again in Section 3.3.2 in relation to the formation of $MoSe_2$ as a secondary phase. By considering the reaction products of Eq. 112 as reactants on the substrate side under corresponding conditions (T_{sub}= 500°C, p = 100 mbar), the calculations further predict the formation of single phase CGSe for a window in the GaCl/CuI ratio in the gas phase between 2.2 and 11([123]. Mixtures of CGSe+Cu_2Se and CGSe+Ga_2Se_3 are expected for lower and higher halide ratios, respectively.

Experimental observations show a general qualitative agreement with the theoretical calculations performed in thermodynamic equilibrium, though deviations from the predicted species and calculated species ratios have been found in actual samples. Clearly, the open-tube CVD system does not strictly operate under equilibrium conditions, and such calculations are only valid when the surface kinetics, both on the source and sample sides, are sufficiently fast. This is usually only the case at high operating temperatures (T>1000°C for the system under study[124]). Nevertheless, equilibrium calculations are of interest *per se* in a double way: firstly, for predicting the formation of gaseous and solid compounds that can be expected to appear in the operation of the system, as well as for determining the active role of the halogen species[38]; and secondly, for determining the extent of dynamic and surface effects in the actual system operation, as inferred from observed deviations from the equilibrium results. These experimental findings will be addressed in the next section.

3.2 Film growth and characterisation

The flexibility of the open-tube system, together with the material tolerance for composition variations (see Chapter 1), allow to grow CGSe films showing large deviations from stoichiometry. Important aspects of the film growth, like its morphology and final thickness, are largely composition-dependent. Furthermore, the electronic properties of the films are severely affected by deviations from the ideal stoichiometry, either to the Ga- or Cu-rich side. In the following, structural aspects of CGSe films as a function of their composition are reviewed, as this point turns out to be critical for the control of the film quality and subsequent processing.

Two parameters are normally used for the compositional characterisation of I-III-VI_2 compounds[35], the cation ratio X and the anion-to-cation ratio Z, given respectively by:

$$X = \frac{[I]}{[I] + [III]} \qquad \text{Eq. 113}$$

$$Z = \frac{[VI]}{[I] + [III]} \qquad \text{Eq. 114}$$

where [*I*], [*III*] and [*VI*] denote the atomic concentration of the corresponding element. Films prepared by CVD systematically show an overall composition with Z≥1, as measured by means of XRF spectrometry analysis, i.e. films contain excess Se

compared to the ideal 1:1:2 stoichiometry. Deviations up to 2 mol% from ideal stoichiometry are found in samples grown on Mo-coated soda-lime glass (SLG), compared to those samples grown on bare SLG reference substrates, as shown in Table 2. These deviations are related to the formation of a Se rich-interfacial layer at the rear CGSe surface, identified as $MoSe_2$, as discussed later. CGSe intra-grain compositions, as measured by EDX point measurements on sample cross-sections shown in the next sections, are only slightly Se-rich, with deviations up to ~0.5 mol% Se-excess in the bulk of CGSe crystallites. Furthermore, by repeating the XRF measurements from the CGSe rear side after lifting off the absorber from the substrate (see Chapter 5), the excess Se is greatly reduced, and values close to stoichiometric Se-content are recovered (see Table 2). As XRF is a *bulk* sensitive characterisation tool in terms of thin-films, surface modifications or composition gradients across the layer thickness accounting for the difference in Se-content can be excluded. Furthermore, Se is found on the substrate side after lifting the absorber off from it, accounting for the difference in Se content from measurements on as-grown and peeled-off samples. No traces of Cu nor Ga are detected on the substrate after removing the absorber. The parameter Z is thus useful for estimating the thickness of the interfacial Se-rich layer from the fit of XRF results, assuming the Se content in CGSe is ~50% and attributing the Se excess to the interfacial $MoSe_2$ layer, as shown in Table 2. The reliability of this procedure has been checked by comparing the predicted thickness derived from XRF analyses of both CGSe and $MoSe_2$ layers resulting from the deposition process, with those values observed in TEM cross-sections of as-grown samples. An agreement between the predicted and experimental thickness within ±15% error has been found in samples showing different cation ratios.

Table 2. Composition of CGSe thin films grown on bare and Mo-coated SLG substrates, as measured by XRF, and corresponding estimated thickness of CGSe and $MoSe_2$. Excess Se in samples grown on Mo (in italics), compared to those grown on glass in the same process, is redistributed in a CGSe/$MoSe_2$ two-layer model. Measurements performed on the same sample after lifting off the absorber from the substrate are also included (last two rows), showing values in agreement with the two-layer model. The experimental error in the determination of the sample composition is estimated in ±0.3% and the corresponding error in layer thickness in ±0.05 µm.

Layer structure	**Fit model**	**Cu mol%**	**Ga mol%**	**Se mol%**	**d(CGSe) µm**	**d($MoSe_2$) nm**
CGSe/SLG	CGSe/glass	23.7	26.0	50.3	0.94	-
CGSe/Mo/SLG	CGSe/Mo/glass	*23.0*	*25.0*	*52.0*	*1.14*	-
	CGSe/$MoSe_2$/Mo/glass	24.0	26.0	50.0	1.09	68
CGSe lifted-off	CGSe/glass	23.9	26.1	50.0	1.05	0
$MoSe_2$/Mo/SLG	$MoSe_2$/Mo/glass	-	-	64.7	-	78

Regarding the cation ratio, a simplified version of Eq. 113 will be cited hereafter, as the [Ga]/[Cu] ratio. Control of the final [Ga]/[Cu] ratio in the solid phase (s) can be achieved by adjusting the corresponding [Ga]/[Cu] in the gas phase (g) during the deposition process, as can be inferred from Eq. 112. For a given source temperature, this is in turn done by controlling the flow of transport gas sweeping the source material boats. Figure 24 shows the correlation between solid and gaseous compositions, where only the external iodine oven temperature, responsible of the Cu transport, was varied. As long as Ga and Se are provided in excess from the Ga_2Se_3 source, it has been found

convenient to adjust the composition by varying the amount of Cu volatilised by reacting with I_2/HI. The [Ga]/[Cu](g) ratio is controlled by weighting the source material boats prior to and after each deposition process. The so calculated mass losses are divided by the molar mass, and further divided by the valence of each cation species in the corresponding compound. The ratio of these quantities gives the cation ratio in the gas phase, as stoichiometric volatilisation occurs from the source boats[122].

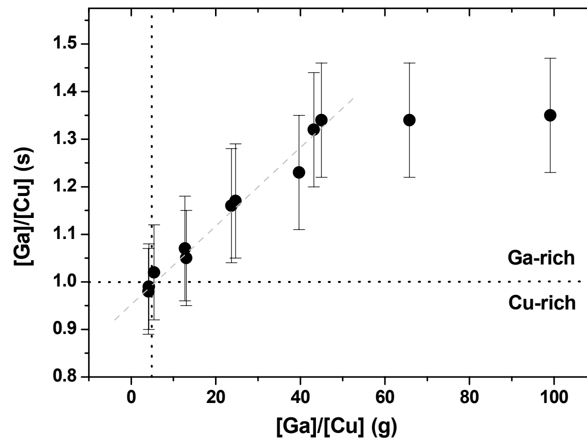

Figure 24. [Ga]/[Cu](s) ratio in CVD-grown CGSe films as a function of the [Ga]/[Cu](g) ratio in the gas phase during the deposition process, as measured by EDX (after Ref. [79]). Dotted lines mark the transition from Cu-rich to Ga-rich compositions. (T_{sub} = 500°C).

Two aspects from Figure 24 deserve some attention:

- A range of linear dependence exists between gas and solid [Ga]/[Cu] contents, up to [Ga]/[Cu](g)~50, marked by the dashed line. CGSe films for PV applications are grown slightly Ga-rich, with [Ga]/[Cu](s) comprised between 1.01 and 1.2. Thus, the control of the film composition can be adjusted via the composition in the gas phase.

- Excess Ga in the gas phase is required in order to grow single-phase stoichiometric CGSe layers ([Ga]/[Cu](g)~5 for [Ga]/[Cu](s) = 1). This aspect was pointed out to be related to the high affinity of I_2 and Ga to form gaseous compounds under typical reactor conditions, as inferred from numerical calculations under thermodynamic equilibrium, and further confirmed by recent electron photoemission studies and first principle calculations[38]. Excess Ga in the gas phase bonds with free I_2 on the sample side, which otherwise may induce either the formation of solid CuI at moderate temperatures (e.g. during cooling down), or back-reactions into the gas phase.

A sharp transition from single phase CGSe to a mixture of CGSe + $Cu_{2-x}Se$ is detected at composition values close to the ideal 1:1:2 stoichiometry. This is a general feature of Cu-containing chalcopyrites[125], further discussed in the next section. The experimental minimum [Ga]/[Cu](g)~5 resulting in single phase CGSe is thus slightly higher than that predicted from thermodynamic calculations in equilibrium, as stated above. No

traces of Ga_2Se_3 have been found on the Ga-rich range of compositions for [Ga]/[Cu](g) values as high as 100, according to XRD and XRF analysis, in contradiction to theoretical calculations. The cation ratio in the solid phase tends to saturate around [Ga]/[Cu](s)=1.35±0.1, according to Figure 24.

The film thickness and crystallite size of Cu-containing chalcopyrite films are functions of their composition. Cu-rich materials show higher growth rates and larger crystallites than Group-III-rich films. Figure 25 shows the exponential dependence of the average film thickness, as determined from weighting the samples after processing and subtracting the weight of the bare substrate, on the [Ga]/[Cu](g) ratio during the deposition process. This method has demonstrated to be accurate down to ± 10% comparing cross-sectional SEM pictures to the average thickness as calculated from XRF analysis of the films. Deviations from the nominal material density of stoichiometric samples with film composition is well below the experimental error up to deviations from stoichiometry in the range of 1:3:5 compounds, validating the procedure based on the sample weight.

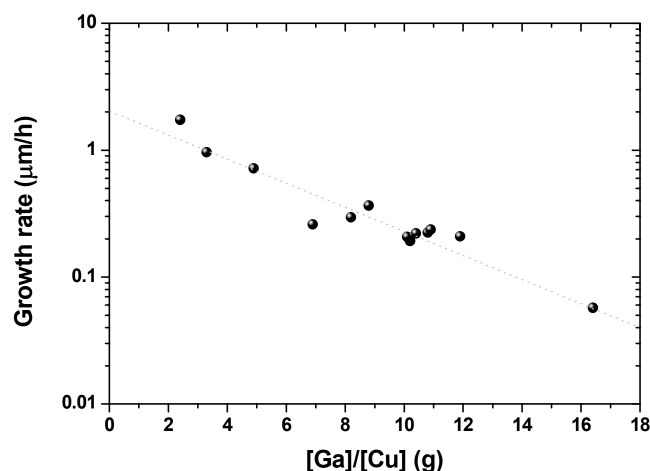

Figure 25. Growth rate of CGSe films in logarithmic scale as a function of [Ga]/[Cu](g). T_{source}=600°C, T_{sub}=500°C, under standard processing conditions (see Appendix I).

Additionally, the crystallite habit and the sample morphology are also composition-dependent. Ga-rich samples are characterised by small triangular grains, as shown in Figure 26 left, with numerous grain boundaries across the film thickness. Similar morphologies have been observed in PVD-grown Ga-rich CGSe films[54]. The average grain size has been determined by quantitative analysis of SEM pictures and further fitted according to a log-normal distribution[79], increasing from 0.6 up to 1 µm with increasing Cu-content in the solid phase between 1.30>[Ga]/[Cu](s)>1.04. On the Cu-rich side, CGSe films show a characteristic polyhedral structure, as shown in Figure 26 right. Closed layers are grown for Cu-rich compositions deviating from the ideal stoichiometry no more than 5%, resulting in non-uniform layers as the Cu-content is increased, as can be seen in Figure 27. The grain size is directly related to the film thickness, as for Cu-rich samples columnar grains develop from the substrate up to the top layer surface.

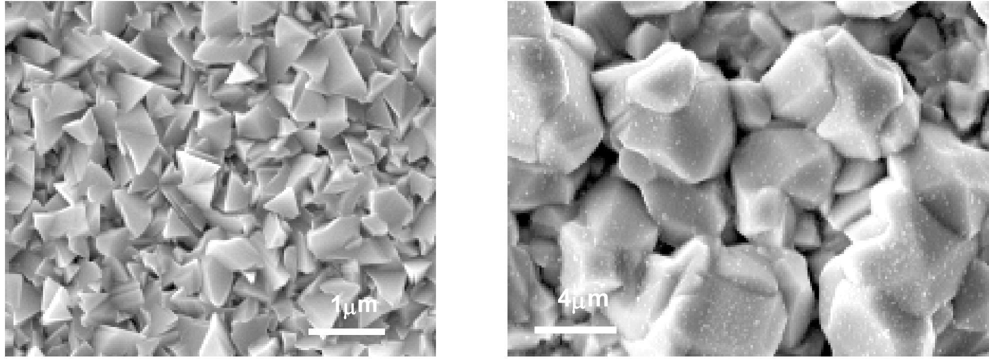

Figure 26. Top-view SEM pictures of a Ga-rich sample [Ga]/[Cu](g) = 11.9 **(left)** and a slightly Cu-rich sample [Ga]/[Cu](g) = 2.5 **(right)**, grown on Mo-coated SLG substrates, showing different crystal habits as a function of their composition.

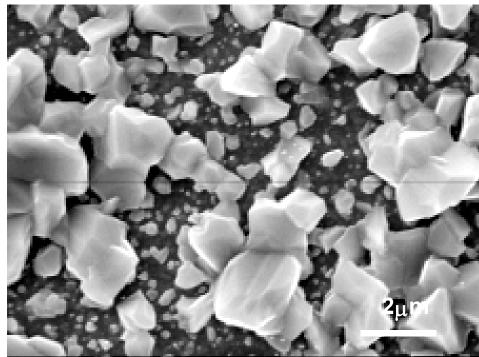

Figure 27. Top view SEM picture of a Cu-rich sample [Ga]/[Cu](g) = 1.5 grown on Mo-coated SLG. Non-homogenous nucleation and incomplete substrate coverage result from largely Cu-rich compositions.

The characteristic morphology and crystal habits of CGSe crystallites as a function of their composition have been explained on the basis of the anisotropy in the <221> direction of the unit cell, which controls the change from polyhedral to tetrahedral crystallites with increasing Ga-content[126]. Metal-terminated {112} planes develop under Ga-rich conditions with the lowest velocity, suppressing the appearance of related chalcogen-terminated planes, and leading to a typical tetrahedral morphology. These predictions have been experimentally confirmed by means of XRD analysis from the increase in the orientation factor $f_{(112)}$ at the transition from Cu-rich to Ga-rich samples[79], resulting from an overall (112) preferential texturing of Ga-rich samples.

Summarising the results shown in Figure 24 and 25, and the remarks on the crystal morphology as stated above and reflected in Figure 26 and 27, some general conclusions can be extracted regarding the composition dependence of the film growth:

- Difficulties are found for the growth of Ga-rich films above [Ga]/[Cu](s) = 1.05, as the growth rate drops down exponentially with increasing Ga content. As an example, with reactor conditions as given in Figure 25, a deposition time well above 10 hours would be required for the growth of a 2μm thick film with [Ga]/[Cu](s) = 1.1.

- Thicker films can be obtained by increasing the Cu-content, up to a rate of nearly 1 μm/h for stoichiometric samples.
- Even higher growth rates (between 1 and 2 μm/h) can be achieved on the Cu-rich range of solid composition. However, films do no longer show CGSe single phase, but a mixture of CGSe and $Cu_{2-x}Se$. Furthermore, an incomplete substrate coverage results from excess Cu-rich conditions, with detrimental effects for subsequent device processing, as discussed in the next section.
- A preferable crystal morphology is shown by samples on the nearly stoichiometric and slightly Cu-rich side of the composition range, with large crystallites of dimensions comparable to the average film thickness, minimising the number of grain boundaries for the electronic transport in subsequent device performance.

Improved PV performance has been achieved from devices based on slightly Ga-rich compositions[127] from PVD processing, and in general, for slightly Group-III-rich compositions in $Cu(In,Ga)Se_2$ chalcopyrite-based solar cells[8]. The same result has been found for CVD-CGSe-based devices[122], resulting from an overall reduction of the density of defect states in the band-gap as the Cu-content is slightly reduced[128], and an improved electronic quality, as discussed in Chapter 4. The dichotomy between a preferable crystalline structure on the one hand (corresponding to slightly Cu-rich compositions) and an improved electronic quality on the other hand (corresponding in turn to slightly Ga-rich compositions) has been resolved by implementing sequential deposition stages during the film growth, yielding high-quality films with typical morphologies of Cu-rich compositions and electronic properties characteristic of Ga-rich samples. The implementation of the sequential deposition approach in the open-tube CVD system will be addressed in Section 3.4. First, in Section 3.3 experimental evidences of the presence of secondary phases in relation to compositional issues of the CGSe growth will be presented and their properties discussed.

3.3 Secondary Phases

Single phase CGSe films can be grown under standard CVD reactor conditions (see Appendix I) for $[Ga]/[Cu](g) \geq 5$. However, various extraneous phases have been found to segregate both in the CGSe film bulk and its surfaces, as inferred from XRD, EDX and KPFM measurements. On the one hand, copper selenides are detected in those samples grown under $[Ga]/[Cu](g) < 5$ conditions. On the other hand, $MoSe_2$ appears as an interfacial layer at the rear contact of films grown on Mo-coated glass. In this section, results are reported on the characterisation of such secondary phases, as they play an important role in further device processing.

3.3.1 Copper selenides

Cu-rich copper selenides of various compositions (see Figure 47) have been found in stoichiometric CGSe samples and in those films grown under Cu-excess. The presence of such phases is in agreement with phase diagrams of the Cu_2Se-Ga_2Se_3 system previously reported[129], which predict little Cu solubility in the CGSe matrix and a wide range of coexistence of both CGSe+$Cu_{2-x}Se$ phases, as shown in Figure 28.

Copper selenides are reported to play a relevant role during the growth of $Cu(In,Ga)Se_2$ materials. Klenk[54] proposed a PVD-growth model for CGSe in which the incorporation of material from the gas into the solid phase is driven by a quasi-liquid $Cu_{2-x}Se$ phase segregated at the film surface. Non-stoichiometric copper selenides show melting points close to standard processing temperatures (~550°C) and thus the solubility of gaseous elements present in the processing chamber is greatly enhanced close to softening-point temperatures of the surface phase. The model satisfactorily predicts the observed large crystallite size of samples grown under Cu-excess, compared to those grown under Ga-rich conditions, as explained above. In addition, it provides the basis for sequential deposition approaches that will be reviewed in the Section 3.4.

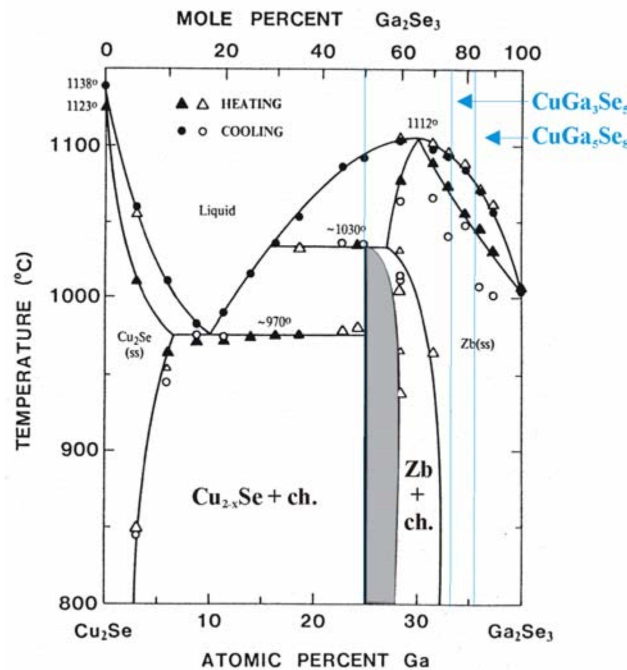

Figure 28. CGSe phase diagram along the pseudobinary cut Cu_2Se-Ga_2Se_3 for T>800°C and at 1 atm (after [129]). The grey marked area denotes the single phase CGSe range. Mixtures of CGSe+$Cu_{2-x}Se$ are predicted for Ga-contents <25at%. Arrows denote compositions of experimentally observed OVCs not reported in [129].

However, the presence of copper selenide segregations in final chalcopyrite films is known to be detrimental for PV applications, due to the degenerated p^+-character these phases systematically show. Nearly metallic shunts are thus available for the electronic transport, if such phases segregate, e.g. as a mesh along grain boundaries or as columnar grains from the rear to the top film surface, ruining the design of the junction when depositing the buffer/window system in contact to it. Wet etching treatments on epitaxially-grown chalcopyrite films, normally based on KCN[130], are required to remove surface layers of $Cu_{2-x}Se$ prior to the buffer layer deposition. However, the wet treatment is insufficient in polycrystalline films if the secondary phase forms entire crystallites, clusters embedded in CGSe crystallites and/or segregations at grain boundaries[131]. All these types of copper selenide secondary phases have been found in Cu-rich CVD-grown CGSe films, as will be shown in the remainder of this Chapter.

As an example of entire crystallites of copper selenide formed during the film growth under Cu-rich conditions, Figure 29 shows a SEM cross-section of a sample grown on a Mo-coated SLG substrate under [Ga]/[Cu](g)=1.5. The white line corresponds to an EDX line-scan shown below, where the Ga-L signal can be seen to remain in the background level throughout the entire layer. Cu and Se are detected in the large polyhedral crystallite, which forms the entire film thickness. Characteristic voids are also visible at the interface between the film and the substrate, revealing the existence of early stages in the nucleation and crystal seed formation of the layer growth dominated by diffusion and surface kinetics, rather than by transport-limited processes[132]. These kinetic effects have been mentioned above to limit the validity of numerical calculations based on equilibrium conditions.

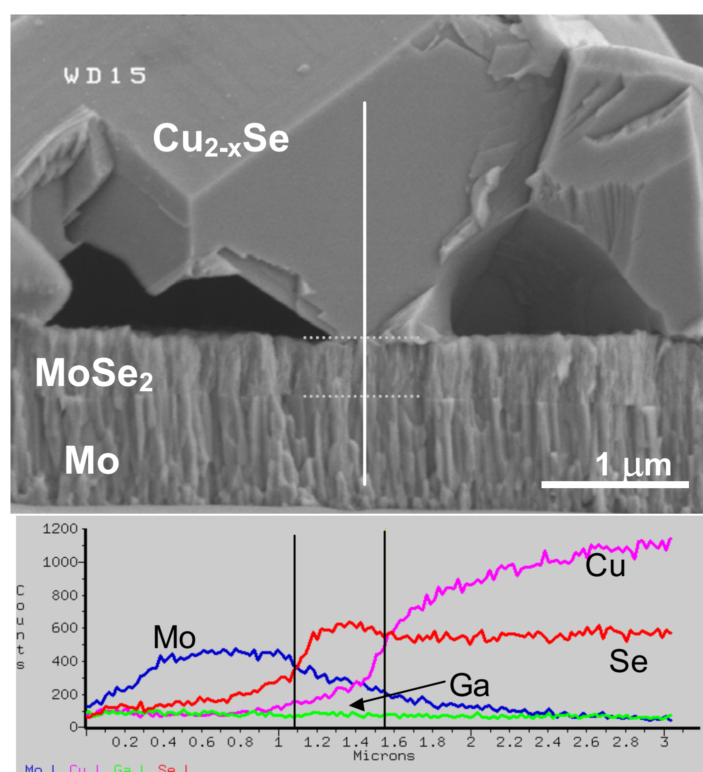

Figure 29. SEM cross-section of a Cu-rich sample. The white line corresponds to the EDX line-scan below. Cu and Se are the main constituents of the crystallite, while Ga remains in the background level. A homogeneous Mo-Se layer is visible between the Mo substrate and the film.

With the aim of elucidating the fundamental reasons for the poor performance of devices based on Cu-rich preparations, CGSe samples showing $Cu_{2-x}Se$ phases were processed as solar cells without any previous chemical treatment, following the standard chemical bath processing for deposition of a CdS buffer and ac-sputtering of a ZnO window layer (see Section 1.3). Cross-sections were subsequently prepared for TEM and KPFM analysis according to the procedure stated in Chapter 2.

Figure 30 shows a SEM picture of such cross-sections. The Cu-foil to be used as reference for the work function calibration is visible as the wide stripe in the centre of the picture, acting as symmetry axis of the face-to-face preparation, with epoxy/window/buffer/absorber/Mo/glass layer sequences on either side. Hollow arrows

point out uncovered substrate zones, characteristic of the incomplete substrate wetting under Cu-rich deposition conditions. At these points, the n-type buffer/window system is found to lie directly on the rear contact, shunting the device. Regions enclosed by rectangles highlight those areas scanned with KPFM, shown later in Figure 34 an 35.

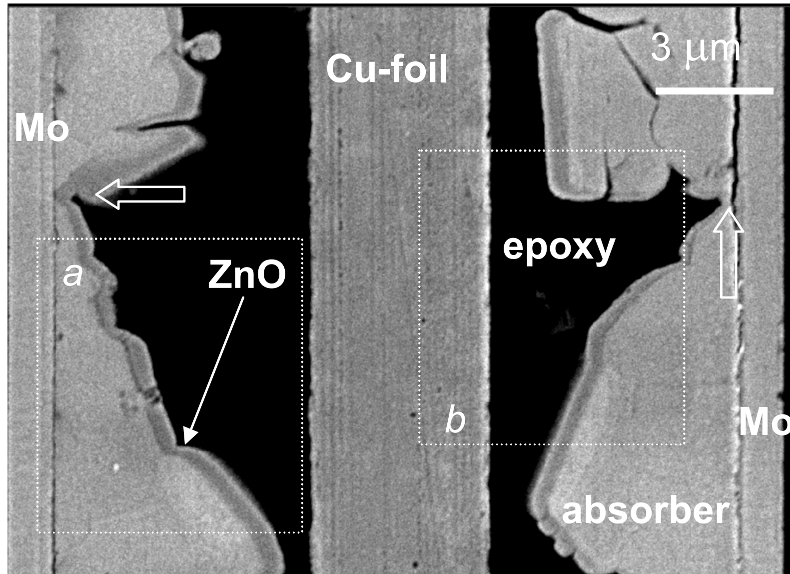

Figure 30. SEM cross-section of a CVD-grown CGSe film, showing the face-to-face sample preparation for KPFM measurements. KPFM scans were performed on the enclosed areas *a* and *b*, shown in Figure 34 and 35. Hollow arrows highlight device shunts on both sides, with the n-type buffer/window directly contacting the rear electrode.

EDX mappings, shown in Figure 31, have been obtained on the same position to help identifying secondary phases. An uneven distribution of Cu and Ga is clearly visible in Figure 31 (a)-(d), showing K and L signals of both elements, indicating the presence of inhomogeneous Cu-rich phases segregated in the CGSe absorber film. The secondary phase consists of large grains of several microns size. Cu-K lines (a) still resolve the shape of the entire film, whereas weaker L-lines (b) sharply limit the boundaries of Cu-rich domains and the Cu-foil. Ga signals (c) and (d) reveal the absence of Ga in those domains of Cu-rich phase. Boundaries appear well delimited in Ga mappings, due to the reduced solubility of this species in copper selenide compounds. It should be noticed that the SEM picture in Figure 30 shows little contrast at the boundaries between these phases. A remarkable contour of the Ga-K line (c) is also visible on the upper part of the sample on both sides of the preparation, corresponding to an overlap with the Zn-K line (h). This is confirmed by the absence of the contour in the corresponding L-line mapping (d). From the Se-L line (e) it can also be concluded that the composition of Cu-rich phases corresponds in turn to a Se-poor compound, compared to the CGSe phase, as deduced from the weaker Se signal on those domains showing Cu-rich compositions with absence of Ga. This is in agreement with the assignment of XRD peaks from secondary phases to Cu-rich copper selenides (see Figure 47).

Comparing the Se (e) signal to those of Cu (a) and Ga (c), it is also noticeable that Se is detected in slightly broader regions closer to the Mo layer (f) on both sides of the preparation. A narrow region of Se and Mo overlapping results when bringing both mappings in a single figure. This is related to the formation of $MoSe_2$ as an interfacial layer between the absorber and the substrate, as commented in Figure 29 and reviewed in the next section.

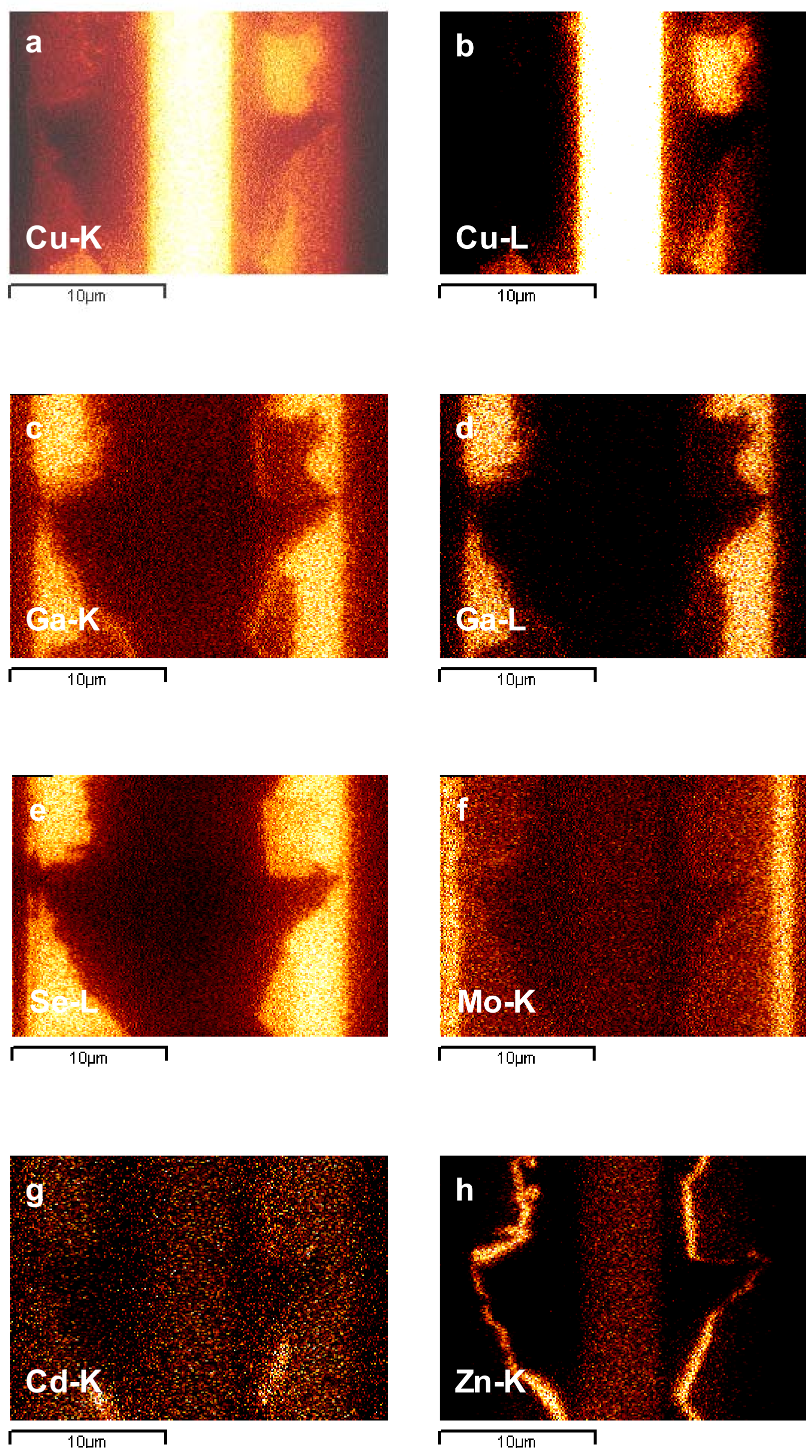

Figure 31. EDX-mappings on the sample cross-section of Figure 30, **(a)** Cu-K, **(b)** Cu-L, **(c)** Ga-K, **(d)** Ga-L, **(e)** Se-L, **(f)** Mo-K, **(g)** Cd-K, and **(h)** Zn-K signals.

Regarding the buffer layer, an inhomogeneous distribution of Cd is found in Figure 31 (g), deserving some attention. It was mentioned previously that the unfavourable electronic properties of $Cu_{2-x}Se$ prevent the formation of operating junctions, and thus removal of the secondary phase prior to the buffer layer deposition is mandatory. However, an ultimate reason for the etching treatment prior to processing of not lesser importance is that the chemical bath normally employed for the CdS buffer layer deposition *does not* provide an efficient buffer layer on non-treated absorbers, but results instead in a closed and homogeneous layer of similar characteristics, whose main components are Cu and S. The structural and electronic properties of copper sulfides are similar to those of selenides[133], and therefore neither one nor the other type of compound provide a convenient buffer for PV applications.

The presence of Cu and S on non-treated layers subjected to CBD processing was revealed by EDX-point measurements performed on the presumed buffer layer during TEM studies of such samples (see Figure 32). These measurements revealed the absence of Cd in large domains of the ~50 nm thick homogeneous layer between the absorber and the window films.

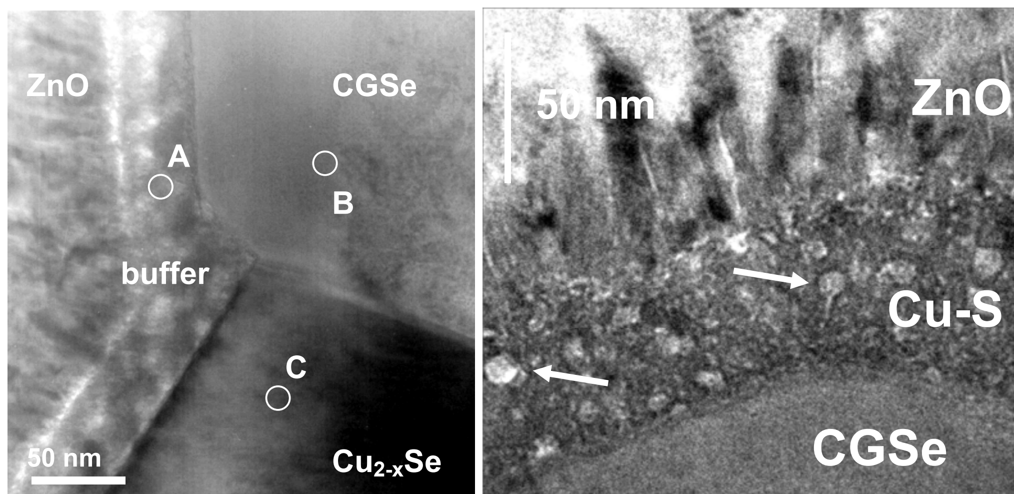

Figure 32. Left: TEM cross-section of the window/buffer/absorber region from a Cu-rich based CGSe solar cell. EDX point measurements on the highlighted spots showed following compositions (±7 at%); **A**: [Cu]=58.1 at%, [S]=41.9 at%; **B**: [Cu]=23.7 at%, [Ga]=24.7 at%, [Se]=51.6 at%; **C**: [Cu]=64.7at%, [Ga]=0.2 at%, [Se]=35.2 at%. **Right:** High-magnification TEM cross-section of the Cu-S 'buffer' layer, showing a characteristic granular structure.

It is proposed that the formation of the closed and homogeneous presumed Cu-S buffer layer during the chemical bath results from a sequential process, involving firstly the removal of the $Cu_{2-x}Se$ surface layer by Cu-complexation with the ammonia contained in the solution, and the subsequent deposition of a Cu-S compound in a similar way as the expected CdS crystallisation from the chemical bath. The fact that both Cu_2S and CuS compounds show a higher stability in aqueous solution than CdS (see Ref. [134]) supports the preferential formation of the copper-containing chalcogenide, if sufficient provisions of Cu and S exist in the solution. The result is the formation of a closed and

homogeneous layer characteristic of the chemical bath processing, with minor incorporation of Cd, as it can be seen in Figure 31 (g).

Nadenau *et al.*[131] reported on the formation of Cd-depleted Cu-S inclusions in the buffer layer of CGSe thin-film solar cells after depositing CdS by chemical bath at elevated temperatures (80°C), from TEM and EDX studies on sample cross-sections. CGSe absorbers were prepared by co-evaporation under Cu-rich compositions and, interestingly, they were subjected to a KCN etching treatment prior to CBD of the buffer layer. Studies on similar samples processed at standard 60°C CBD showed no traces of copper sulfides within the buffer, leading the authors to conclude that higher bath processing temperatures enhance the reactivity between the absorber and the deposited buffer. Additionally, copper selenide precipitates were found in the near surface region of the etched CGSe samples, likely acting during the CBD process as a reservoir for out-diffusing Cu, and additionally demonstrating the limited efficacy of the etching treatments. These results can be interpreted in the frame of the sequential process stated above, starting with a Cu-complexation stage from the out-diffusing Cu originated in the copper selenide precipitates, and its subsequent deposition in the form of copper sulfides, as the amount of sulfide in the solution increases from the decomposition of the thiourea during the warming-up of the chemical bath.

The formation of a Cu-S compound instead of the expected CdS buffer layer has additionally been reported by Kazmerski *et al.*[135] and Niemi and Stolt[136] on $CuInSe_2$ absorbers of Cu-rich compositions, as determined from XPS and Secondary Ion Mass Spectroscopy (SIMS) mappings on samples prepared by co-evaporation and studied *in situ*. In Ref. [136], Cu-S was reported to form nodules of 5-15 nm diameter, in agreement with the granular structure found in Figure 32. Cd and S were evaporated in these studies, thus excluding the participation of complexing agents that may contribute to the removal of the surface chalcogenide layer, as previously suggested, and the subsequent recrystallisation from the solution. Therefore, a single stage process leading to the deposition of Cu-S clusters, likely based on certain degree of chalcogen exchange (release of Se and incorporation of S into the binary compound), cannot be excluded from those results during dry processing of the buffer layer. Such interchange of chalcogen species has been reported between device-grade $Cu(In,Ga)Se_2$ (i.e. excluding the presence of $Cu_{2-x}Se$ phases) and the CdS buffer deposited by chemical bath[137], but the conclusion of that work pointed to the formation of $Cu(In,Ga)(S,Se)_2$ (i.e. incorporation of S into the chalcopyrite matrix), and no traces of the binary compound were found. However, a simple chalcogen intermixing reaction cannot explain the typical morphology, including the expected film thickness, of the presumed buffer shown in Figure 32, only attributable to a chemical-bath-based deposition.

KPFM measurements were performed on the sample shown in Figure 30, prior to SEM and EDX analysis. The sample was mounted in the UHV chamber of the KPFM system right after preparation, showing a reduced contact potential difference between sample constituents, including the metallic Cu-stripe embedded in the conductive epoxy during the face-to-face preparation. Mechanical polishing and subsequent cleaning in air are expected to result in sample surfaces covered with adsorbates, which may severely alter their electronic properties. In particular, differences in work function between different constituents of the samples fade away under the ubiquitous presence of adsorbed water vapour and carbon dioxide, as such adsorbates greatly reduce the free energy of any surface exposed to air[133], constituting a general matter of concern of surface-sensitive

characterisation techniques. An *in-situ* cleaning process compatible to UHV conditions is thus required for samples which have been exposed to air, with the major constraint of being (ideally) inert against sample damage or modification. In practice, only approximations to this cleaning process exist, mostly based on soft ion-sputtering, normally performed with Ar or N ions. The degree of surface damage on the sample under study is directly related to the energy of the ions and the incident angle subtended between the ion source and the sample surface[138]. According to these considerations, a cleaning process based on soft sputtering was optimised for the application of KPFM on samples that have been prepared in air[139].

The sample was first annealed 1 hour at 110°C to desorb water, and subsequently subjected to soft sputtering/annealing cycles, monitoring the evolution of the measured work function on the cleaned surface at each step. The results are summarised in Figure 33. Sputtering steps of 5 to 10 minutes were performed with Ar^+ ions at 500 eV under 45° incident angle. It was found that a minimum sputtering time of 15 minutes under these conditions was necessary to discern differences in contact potential between sample constituents. The Cu stripe included in the face-to-face preparation proved to be helpful in monitoring the progress of the cleaning procedure. Further details on the sputter-cleaning process can be found in Ref. [140].

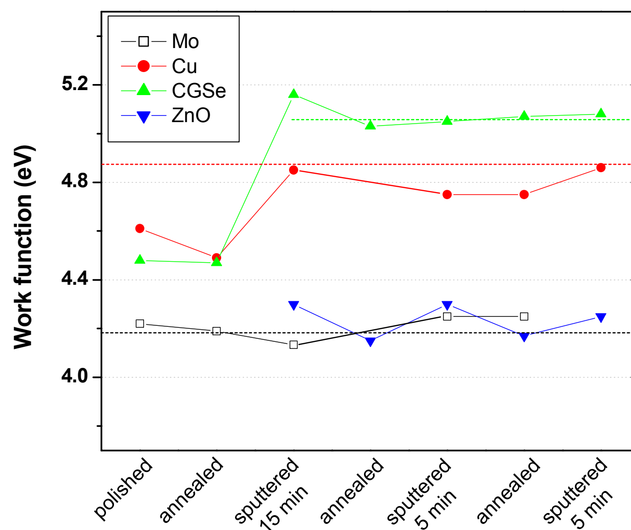

Figure 33. Evolution of work function values at various positions of different constituents of the cross-section. Dashed lines denote reference Φ values for Cu and Mo, as well as the average Φ value measured on CGSe phases. Little contrast in Φ values is visible prior to ~15 min sputtering. Subsequent short sputtering/annealing cycles do not result in significant changes.

After proceeding with the cleaning process, KPFM measurements reveal the appearance of secondary phases, not only as those crystallites in the absorber film that can be seen in the EDX-mappings of Figure 31, but also as a surface layer segregated both at the top surface and along grain boundaries of CGSe crystallites. Figure 34 and 35 show work function mappings, as measured with KPFM after a total sputtering time of 1 hour in steps of 5-10 minutes and a total annealing time of 3 hours at 110°C, on those marked areas of Figure 30. The colour scale reflects differences in the work function, after rescaling contact potentials into absolute work function values by calibrating the work

function value of the tip on a highly-oriented pyrolytic graphite (HOPG) reference sample. A clear contrast is obtained between the ZnO and the absorber films, and between different phases present in the latter. Comparing Figure 34 and 35 to Figure 30 and 30, it is concluded that $Cu_{2-x}Se$ phases correspond to domains of high work function, with Φ_{Cu-Se}~ 5.35±0.02 eV.

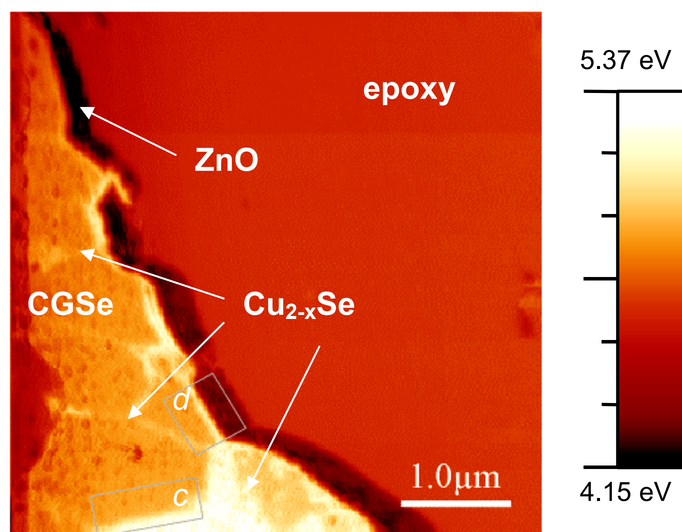

Figure 34. Work function mapping from KPFM scans on the cross-section presented in Figure 30 (*a*). High work function phases (bright) correspond to $Cu_{2-x}Se$ segregations, forming crystallites (at the bottom) and surface layers along CGSe crystallites (medium contrast) and grain boundaries. ZnO shows the lowest work function values in accordance to its n^+ character. Enclosed areas *c* and *d* refer to Figure 36 and 37, where average work function line-scans have been calculated.

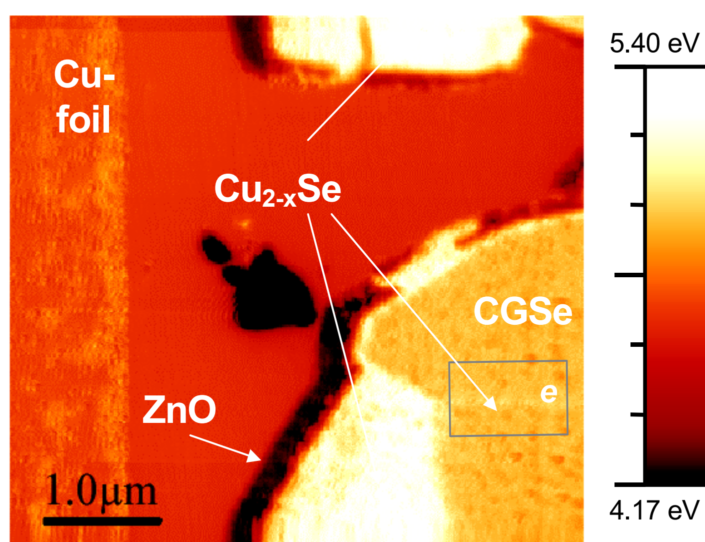

Figure 35. Work function mapping from KPFM scans on the cross-section presented in Figure 30 (*b*). The enclosed area *e* refers to Figure 38, where the work function change across the grain boundary, visible as a bright line, is monitored in an averaged line-scan.

Figure 36 to 38 show values of the work function after averaging a number of line-scans (between 50 to 98 in different positions) in those regions *c*, *d* and *e* of Figure 34 and 35 enclosed by rectangles. Figure 36 shows the work function change recorded at the interface between CGSe and $Cu_{2-x}Se$ crystallites measured in darkness and under He-Cd laser illumination (λ=442 nm, P~60 mW), together with the corresponding surface photovoltage in saturation ($SPV=\Phi_{illum}-\Phi_{dark}$). $Cu_{2-x}Se$ shows a constant work function value independent of illumination, characteristic of a metallic behaviour. Average values of the work function of 5.02±0.02 eV were obtained for CGSe in darkness and 5.09±0.02 eV under super-band gap illumination. A positive SPV is expected for p-type semiconductor samples, indicating a downwards surface band bending in dark conditions as result of the presence of ionised donor-like surface states. These results are in agreement with previous KPFM measurements carried out on the top surface of CGSe samples grown on different substrates, which are summarised in Table 3. It should be mentioned that measurements performed on cross-sections subjected to the cleaning process based on series of sputtering/annealing cycles as explained above, yield comparable values of the work function and surface photovoltage to those obtained on samples transferred from the preparation chamber to the KPFM system in inert gas. This observation supports the realisation of cleaning processes on samples exposed to air, though careful monitoring on the evolution of measured values as shown in Figure 33 should be carried out in any case.

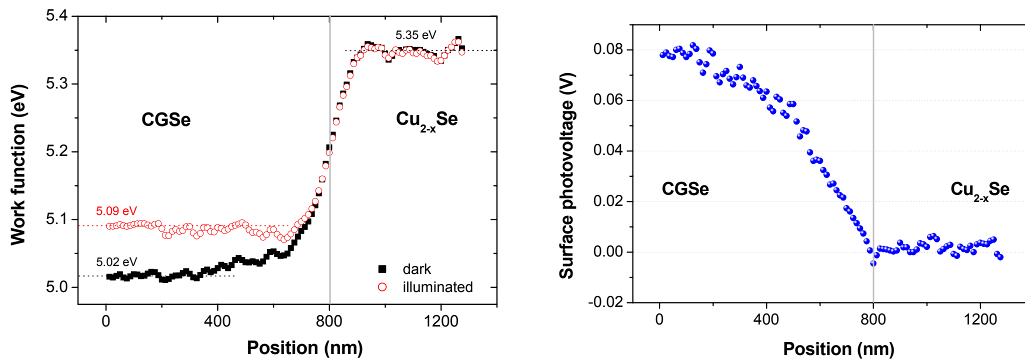

Figure 36. Averaged line-scan of the work function at the interface CGSe/$Cu_{2-x}Se$ indicated in the box *c* of Figure 34 in darkness and under illumination **(left)** and corresponding surface photovoltage **(right)**. The vertical line at ~800 nm denotes the electronic junction, as inferred from the maximum value of the electric field (maximum slope of the contact potential CP profile, as E=dCP/dx) and the SPV constancy on the $Cu_{2-x}Se$ side up to this position.

Figure 37 shows the average work function across the active p-n junction between the CGSe absorber and the ZnO window layers on the area *d* depicted in Figure 34. The position of the presumed buffer layer is indicated by the arrows, corresponding to the hill found in the work function profile across the p-n junction. No electronic differences between copper selenides and sulfides could be found from KPFM analysis, and the presence of a Cu-S compound conforming the presumed buffer is assumed, based on the TEM/EDX results shown before. Translating the work function profile to the conduction band line-up of the heterostructure (and here a metallic character is assumed for the Cu-S phase) a potential barrier of ~200 meV is inferred from this figure for free

electrons diffusing from the absorber to the front electrode, constituting an additional inconvenience for the electronic transport of such structures.

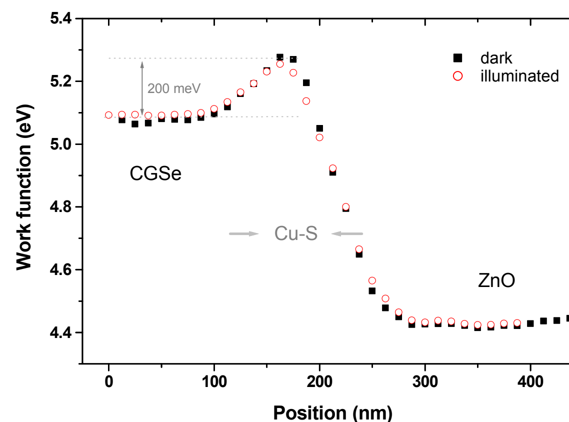

Figure 37. Averaged line-scan of the work function at the interface absorber/buffer/window, box *d* in Figure 34. A non-favourable band line-up is inferred at the absorber/buffer interface resulting from the upwards band bending, in the transit from the absorber to the window layer, constituting a barrier for minority carrier injection to the n-side.

Figure 38 shows the averaged work function measurements across the grain boundary between two CGSe crystallites, in the box marked *e* in Figure 35. $Cu_{2-x}Se$ is presumed to be segregated at the boundary, accounting for the ~140 meV upwards band bending inferred from the measurement in the dark. Opposite results have been found[141] on grain boundaries of PVD-grown CGSe, where the work function was found to decrease by 110±24 meV, and on CVD-grown samples with Ga-rich compositions, as shown in Section 5.2.2. A reduced lateral resolution, as result of zooming from the 5x5 μm^2 scan of Figure 35 to a reduced area of ~280x500 nm^2 over which the average of line-scans leading to Figure 38 was performed, likely limits the absolute value of the work function right at the grain boundary, which should amount up to ~5.35 eV, according to the value of the $Cu_{2-x}Se$ phase in Figure 36. This is due to the smearing effect of sharp features contributing to the mean electrostatic force experienced by the tip/cantilever system, largely wider in comparison to narrow sample boundaries, as reviewed in [142].

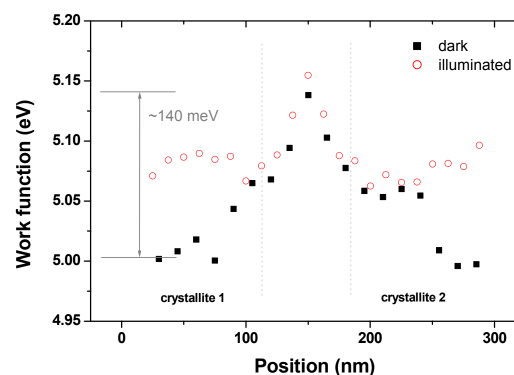

Figure 38. Averaged line-scan of the work function across the grain boundary between CGSe crystallites highlighted in the box *e* in Figure 35.

Table 3. Work function Φ and SPV results from KPFM measurements reported in the literature on CGSe samples, including results on cross-sections prepared in air and subjected to the cleaning process based on soft sputtering and annealing cycles from this work. Particular CGSe lattice planes could be identified in certain cases from geometrical considerations based on the topography of as-grown samples[143]. Illumination conditions (power and wavelength of the laser source) are included with the SPV data when reported. Sample composition and transfer conditions to the KPFM set-up are also commented.

Samples	**Plane**	**Φ(eV)**	**SPV(V)**	**Comments**	**Refs.**
CGSe/ZnSe(110) MOCVD	$\bar{1}\bar{1}\bar{2}$	**5.06**	-	Transferred in inert gas	143
	112	**4.87**			
	102	**4.87**			
	111	**4.84**			
CGSe/ZnSe(110) CVD	204	**5.29**	-0.36 (5 mW, 675 nm)	Ga-rich transferred in inert gas	144
CGSe/Mo/glass CVD	$\bar{1}\bar{1}\bar{2}$	**5.47**	-	Transferred in inert gas	143
	112	**5.3**			
	110	**5.21**			
CGSe/Mo/glass CVD		**5.53**	0.08 (20 mW, 675 nm)	Stoichiometric, transferred in inert gas	144
CGSe/Zn:GaAs MOCVD		**5.1**	-0.30 (675 nm)	Cu-rich	145
		5.4	0 (675 nm)	Etched, transferred in air	
CGSe cell cross section CVD		**4.96**	0.04 (60 mW, 442 nm)	Ga-rich, Ar-sputtered 500 eV + annealing	This work
CGSe cell cross section CVD		**5.02**	0.08 (60 mW, 442 nm)	Cu-rich, Ar-sputtered 500 eV + annealing	This work

The extraction of reliable quantitative information on CGSe net doping concentration from these measurements is not an easy task, as long as two-dimensional information is contained in Figure 36-38. On the one hand metallurgical junctions, e.g. that between CGSe and $Cu_{2-x}Se$ shown in Figure 36, are expected to result in a depletion region on the lightly doped side of the junction, as explained in Chapter 1. The energy band bending associated to the existence of a depletion region (and additionally any possibly related conduction band off-set) are measured by KPFM as a change in the sample work function, as the Fermi level (assumed to be constant under equilibrium conditions) approaches or moves away from the vacuum level through the SCR. This effect is clearly seen in Figure 36-38. However, an additional surface band bending overlaps that bending resulting exclusively from the existence of the junction, the former being related to the SPV value, as shown schematically in Figure 39. Simulations of this effect have been reported[146] on measurements performed on cross-sections of a GaP p-n junction. In the following, it will be assumed that the entire contribution of the surface band bending to the global change in work function corresponds to the SPV value far from the junction. In other words, flat band conditions are presumed under illumination, and no Fermi level pinning (e.g. due to a high density of surface states or a high surface recombination velocity of minority carriers) prevents the surface to behave electronically like the bulk. This crude statement is somehow ambiguous: the photosaturation criterion for stating flat band conditions requires sufficient super-band gap illumination intensity, creating sufficient photoexcited carriers that can screen the surface charge[147]; but a high illumination intensity brings the semiconductor far from

equilibrium and the constancy of the Fermi level cannot be maintained due to the splitting of the quasi-Fermi levels of majority and minority carriers, as stated in Chapter 1. Furthermore, in order to obtain a relationship between the surface band bending and the excess carrier density from charge neutrality principles, it is necessary to assume the constancy of the quasi-Fermi levels through the surface depletion region[115], and this is only the case if defect-related recombination currents can be neglected in first approximation. If this is the case for the samples under study (after undergoing sputtering cycles) is, at least, doubtful. Nevertheless, such an approximation will be adopted, under the premise that values of the net doping concentration derived from it shall be considered only approximated.

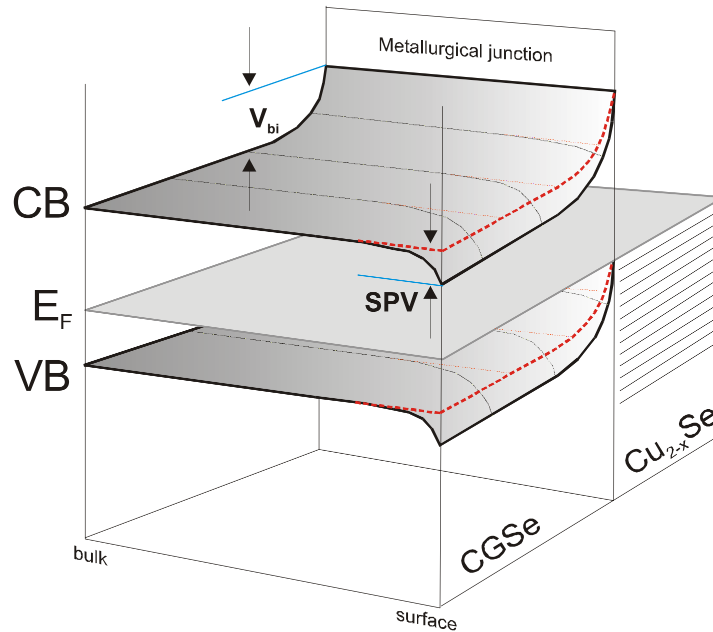

Figure 39. Schematic 2-dimensional energy-band diagram (CB = conduction band, VB = valence band, E_F = Fermi level) of the CGSe/$Cu_{2-x}Se$ junction, after the work function line-scan of Figure 36, showing the contributions to the overall band bending from the junction built-in potential (V_{bi}) and from the surface photovoltage (SPV).

Following Eq. 16 (see Chapter 1), the net doping concentration on the CGSe side of Figure 36 can be estimated from its relationship with the depletion region associated to the junction and the voltage drop across it. The voltage drop ΔV associated to the junction corresponds to the change in Φ/q measured between both compounds. The space-charge region width w extends from the electronic junction to the position where a constant Φ value is achieved on the CGSe side, which is assumed to correspond to the bulk value under high intensity illumination conditions. From Figure 36, ΔV=0.26 V, w=130 nm, and ε~10 is assumed from the literature[148]. Substituting values:

$$w = \sqrt{\frac{2\varepsilon\varepsilon_0 \Delta V}{q N_{eff}^{abs}}} \Rightarrow N_{eff}^{abs} \approx 2 \cdot 10^{16}\, cm^{-3} \qquad \text{Eq. 115}$$

The value obtained for the effective doping concentration on the CGSe side lies in the expected range, compared to doping concentrations on PVD-grown CGSe films from quantum efficiency analysis on processed layers ($N_{eff}^{abs} \sim 5.2 - 6.5 \cdot 10^{16}$ cm^{-3}, from[149]).

3.3.2 Molybdenum diselenide

$MoSe_2$ has been found to form an intermediate layer between the CGSe absorber and the rear contact in samples grown on Mo-coated glass (see Figure 29). XRD measurements on such samples show additional peaks to those from CGSe and Mo, as can be seen in Figure 40, which are assigned to 2H-$MoSe_2$ (JCPDF card number 29-0914). The remarkable structural properties of this compound are briefly reviewed in the following, as they provide the basis for the lift-off process addressed in Chapter 5.

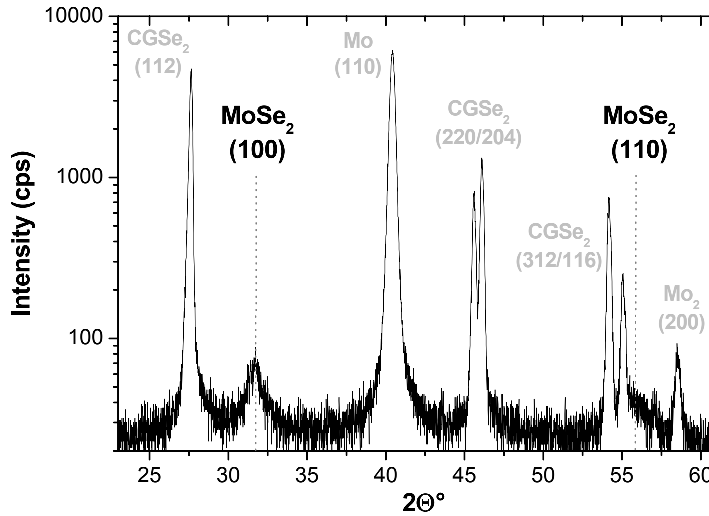

Figure 40. XRD diffractogram of a CGSe sample grown on a Mo-coated SLG substrate. Peaks are labelled according to JCPDF 29-0914 (2H-$MoSe_2$), JCPDF 42-1120 (Mo) and JCPDF 35-1100 (CGSe).

Molybdenum diselenide is a semiconducting material which belongs to the class of compounds known as transition metal dichalcogenides, most of which form layered structures, similar to the case of graphite[150]. The term *layer* refers in this context to the existence of parallel lattice planes in these compounds showing a remarkable anisotropy in both their structural and electronic properties.

The crystalline structure of $MoSe_2$ consists of hexagonal planes. The repeating two-dimensional unit is a slab formed by a plane of Mo atoms in between two planes of Se atoms. The metal atom is always coordinated by six chalcogens, leading to a trigonal prismatic geometry. Two polytypes have been reported for $MoSe_2$, the most common $2H_b$ and the 3R structures[151], which differ from each other in the stacking sequence, shown schematically in Figure 41. In the $2H_b$ polytype, the stacking follows the sequence BcB AbA, (upper caps for chalcogen, lower caps for metal). The two adjacent Se-Mo-Se slabs in the unit cell are laterally displaced with respect to each other,

resulting in the Se atom of the upper sandwich laying directly above the Mo atom of the lower sandwich. On the other hand, the 3R polytype is characterised by three Se-Mo-Se slabs in the unit cell, with a stacking sequence BcB CaC AbA.

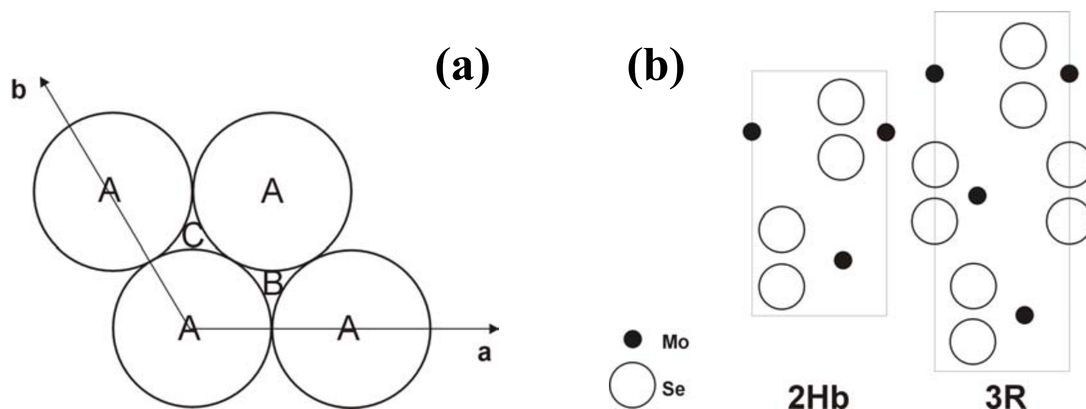

Figure 41 (a) Lattice section along the (001) plane, with atomic positions for the stacking sequence indicated. (b) $2H_b$ and 3R polytypes of $MoSe_2$ represented by the projections on the (110) plane. Adapted from [152]

Interactions between atoms in a slab are mainly covalent, while only saturated orbitals of the chalcogen are exposed outwards from the plane. Slab-to-slab interactions are therefore governed by much weaker processes than the strong covalent bonding within a given slab, and are normally referred to as of the van der Waals type[153]. For this reason, the layers building up the compound are commonly cited as *van der Waals planes*. The weak interaction between van der Waals planes permits in turn to cleave crystals of layered compounds easily along the basal plane.

This different bonding character (intra- vs. inter-planar) in the layered compounds is responsible for the high anisotropy of a number of physical parameters and leads in turn to some peculiarities which characterise these materials. As an example, the electrical conductivity differs by some orders of magnitude when considering the electronic transport along or across the van der Waals planes[154]. This is due to the fact that charge carriers are localised within individual layers, thus behaving as if moving through a stack of independent layers[155]. Additionally, the chemical reactivity of the compound is almost exclusively confined in the plane of the growing layer, the van der Waals planes being to a large extent chemically inert. The relative orientation of the layered compound at a given interface with a different material will therefore determine their satisfactory or poor adhesion, a fact that will control the realisation of lift-off processes, as discussed in Chapter 5. For these reasons, the arrangement of the $MoSe_2$ as an interfacial layer between the active absorber layer and the rear contact of the solar cell will be critical for the device performance, as long as both the adhesion to and electronic transport across this intermediate layer will depend on the disposition of the layers building up the compound.

$MoSe_2$ developed under operating conditions during the growth of CVD-CGSe consists of polycrystalline films of variable thickness (10-200 nm), as inferred from XRD and TEM analyses. This interfacial layer accounts for the Se excess found by XRF

spectrometry in CVD-grown CGSe samples on Mo-coated glass substrates, as discussed in Section 3.2. TEM studies were performed on cross-sections of complete solar cells revealing the structural arrangement of the $MoSe_2$ with respect to the surface planes of the Mo substrate and the CGSe. An overview image and two high-resolution pictures of the $MoSe_2$ layer are shown in Figure 42.

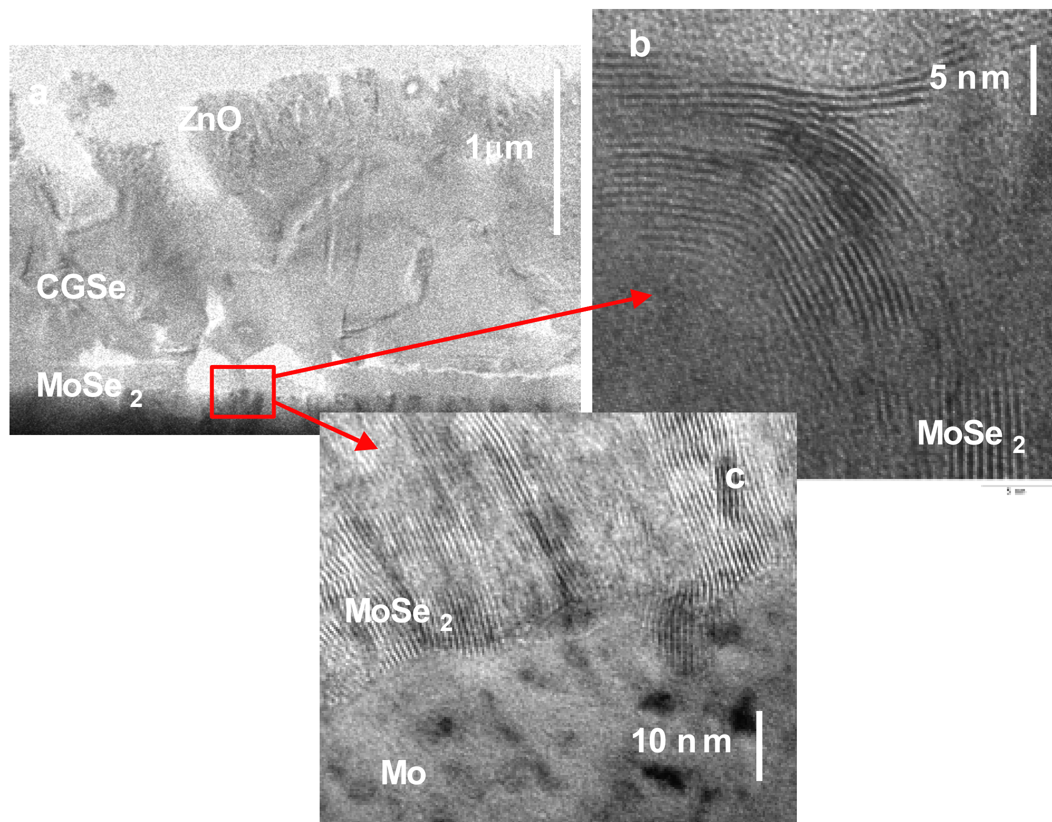

Figure 42. TEM cross-section of a complete solar cell **(a)** and high-resolution shots at the $MoSe_2$ interfacial layer. **(b)** Uppermost region of $MoSe_2$, showing type II (parallel) orientation with respect to the CGSe rear surface (not visible, above). **(c)** Mo/$MoSe_2$ interface, where $MoSe_2$ develops a type I (perpendicular) orientation with respect to the Mo surface. The layered structure corresponds to Se-Mo-Se slabs, separated by ~6.5 Å, in accordance to 2H-$MoSe_2$.

$MoSe_2$ forms a closed and homogeneous interface with the Mo substrate, as already pointed out in Figure 29. Trenches are nonetheless visible in Figure 42 (a), attributed to polishing damage during sample preparation. At this interface, the basal planes of $MoSe_2$ are perpendicularly oriented with respect to the Mo surface, in what hereafter will be referred to as *type-I* orientation of the $MoSe_2$, as revealed in Figure 42 (c). This orientation is found along the entire layer thickness, except in numerous domains at the uppermost part (last 15-25 nm), where a peculiar rearrangement of the planes takes place, as seen in Figure 42 (b), recorded as a progressive bending of the basal planes in nearly 90°. Resulting from the bending, a change from type I to *type II* orientation (with van der Waals planes parallel to the surface) occurs in the proximity of the $MoSe_2$/CGSe interface. The area ratio between type I and type II domains determines the quality of the interface, as discussed above. Additionally, the existence of type II domains is held responsible of the systematic CVD-CGSe absorber peeling found in

samples subjected to KCN etching treatments. The active etching agent presumably attacks the layered compound via intercalation processes, which result in the breakage of the weak van der Waals bondings. Such reactions are unlikely to occur across the basal planes, due to the chemical inertness of the compound along these surfaces.

Three main factors have been found to play a role in the formation and development of the $MoSe_2$ interfacial layer under CVD operating conditions: the Na-content of the glass substrate; the composition of the gas phase during the growth of CGSe films; and the conditioning of the Mo substrate. From these experimental evidences, it can be concluded that the formation of $MoSe_2$ during the CVD processing of CGSe absorbers does not result from simple substrate selenisation, but from the combination of complex processes taking place simultaneously on the substrate surface.

3.3.2.1 Sodium content

The importance of Na in the growth of I-III-VI_2 chalcopyrite absorbers for PV applications is well established from experimental results[66,67]. The alkali metal promotes a large crystallite growth, increases the net doping concentration of otherwise highly compensated Group-III-rich absorbers, and likely participates in the surface and grain boundary passivation together with oxygen. Experimental evidence has also been found of Na segregation on the absorber films right after the deposition process[50]. Na diffuses from the glass substrate through the Mo rear contact into the absorber layer, and from there it tends to concentrate at interfaces. Na-precursors are used in industrial growth of chalcopyrite absorbers for solar cells, together with diffusion barriers on the glass substrate, in order to carefully control the total amount of alkali in the final layer[156].

Relatively large amounts of Na (in concentrations likely exceeding 10^{19} cm^{-3}, as inferred from XPS studies on the CGSe top surface[50]) are thus available at the Mo top surface at processing temperatures (typically 500°C) right before the actual absorber deposition starts. CVD processes have been realised for the growth of CGSe on Mo-coated glass substrates, using both Na-containing and Na-free glass types. Both types of samples have shown $MoSe_2$, as inferred from XRD and XRF analysis after processing, with similar structural properties. As-grown CGSe films show a clear difference regarding the type of substrate employed. Films grown on Na-free glass substrates peel off themselves easily from the Mo substrate, simply by the effect of the electrostatic force induced by touching the polyethylene box where samples are stored. This fact points to a weak adhesion between the CGSe absorber and the Mo contact in samples grown on Na-free glass substrates, likely resulting from a dominant type II orientation of the interfacial $MoSe_2$ layer at the metallurgical junction with the absorber. Contrarily to this case, a satisfactory adhesion is found in those samples grown on Na-containing glass substrates.

Figure 43 shows SEM images of the rear surface of CGSe absorbers grown on Na-free and Na-containing glass. The CGSe sample grown on Na-free glass peeled off itself from the substrate in the polyethylene box. The sample on Na-containing glass was peeled off following the procedure described in Chapter 5. Both samples show the characteristic morphology of Ga-rich compositions (see Figure 26 left), with numerous voids and hollow structures randomly distributed among the tetrahedral CGSe crystallites. Comparing with the top view shown in Figure 26, well defined tetrahedrons visible from the rear side are inferred to have developed freely, whereas regions with irregular shapes are attributed to contact areas with the substrate. From this observation,

a different density of contact areas (with few examples marked in Figure 43) is found when comparing both rear-view pictures. Regions of intimate contact between CGSe and $MoSe_2$ can only result from domains of type I orientation of the layered compound, whereas weak van der Waals interactions do not presumably provide a high sticking coefficient for the nucleation of CGSe seeds on the selenised substrate. It is thus concluded that Na diffusing from the glass substrate has a direct influence on the ratio of type I to type II domains, providing a satisfactory adhesion for the growth of CGSe on Mo-coated SLG substrates.

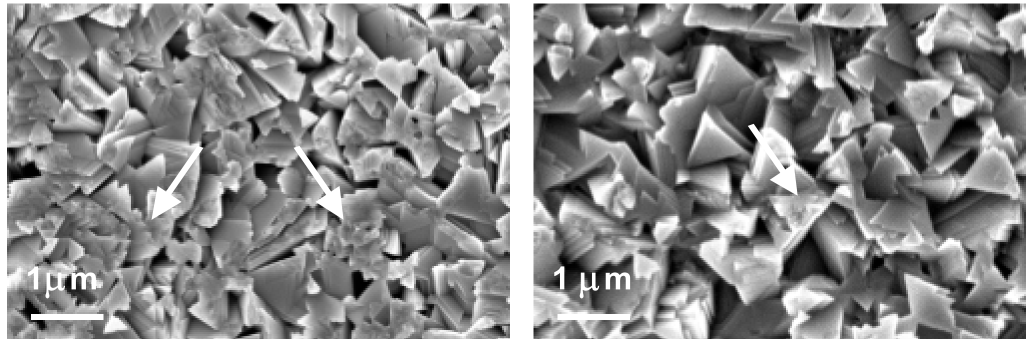

Figure 43. SEM pictures of the CGSe rear surface from samples grown on SLG **(left)** and Na-free glass **(right)**. The density of contact areas (irregular and rough domains) with the substrate is reduced in the case of Na-free glass. For these samples a higher ratio of Type II orientation of $MoSe_2$ at the interface is inferred.

3.3.2.2 Gas phase composition

The formation of $MoSe_2$ in the presence of reactive gases responsible of CGSe deposition has been analysed in a series of CVD processes where the two lines of Cu_2Se and Ga_2Se_3 source materials were operated separately. Mo-coated SLG substrates were subjected to annealing processes at T_{sub}= 500°C under Ga_xCl_y and H_2Se flows during 45 minutes and 4 hours in a series of runs, and under CuI and H_2Se flows during 2 hours with T_{Iodine}= 60°C and 70°C in a second series of processes, with other parameters as in standard CGSe processing (see Appendix I). Samples were analysed by means of XRD and XRF. Figure 44 shows XRD diffractograms from two pairs of samples from each series of processes.

Samples annealed under Ga_xCl_y/H_2Se during 45 minutes and 4 hours show characteristic peaks of 2H-$MoSe_2$, in addition to those from the Mo substrate. No formation of Ga_2Se_3 can be concluded from the XRD results. Both diffractograms show similar features and comparable peak intensities. In particular, peaks corresponding to type I (h,k,0) and type II (0,0,l) orientations are present. An additional broad signal attributed to mixed type character (h,k,l) close to 2θ~38° is inferred to correspond to the transition region of progressive bending from type I to type II orientations, shown in Figure 42 (b). The full $MoSe_2$ structure, including the characteristic bending, found as an interfacial layer between the CGSe absorber and the Mo rear contact can thus be reproduced without the actual presence of CGSe on the substrate, just by annealing the Mo substrate under a gaseous mixture of Ga_xCl_y and H_2Se. This result excludes the

eventual participation of the developing CGSe film in the change from type I to type II orientation, e.g. by inducing strain on the $MoSe_2$. The bending appears, on the contrary, as an intrinsic feature resulting from the interaction of the reactive gases with the Mo surface.

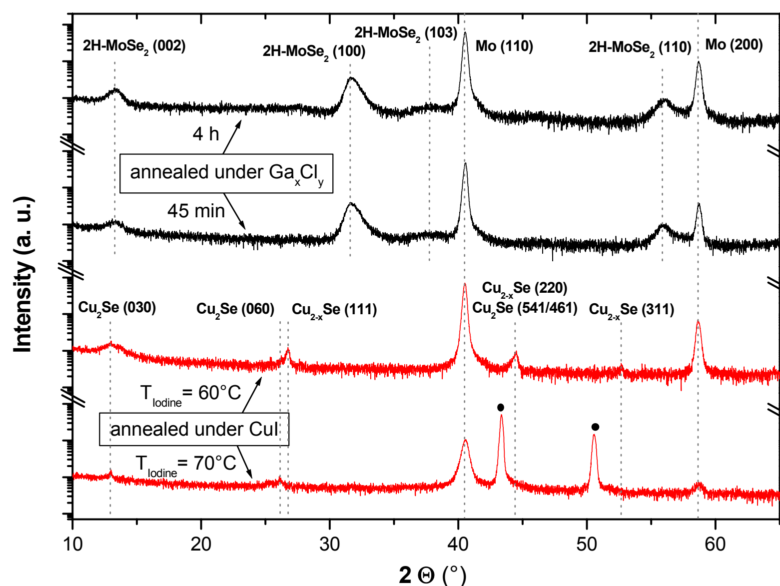

Figure 44. XRD diffractograms of Mo-coated SLG substrates subjected to Ga_xCl_y/H_2Se and CuI/H_2Se gaseous flows. $MoSe_2$ peaks are observed in samples annealed under Ga_xCl_y/H_2Se, whereas copper selenides are found on samples annealed under CuI/H_2Se. Additional Cu peaks (•) appear with high Cu-content in the gas phase (T_{Iodine}= 70°C).

Samples annealed under CuI/H_2Se apparently do not develop $MoSe_2$ under standard flows employed for the growth of CGSe. Additional peaks to that characteristic of the Mo substrate are attributed to copper selenide phases Cu_2Se (JCPDF 37-1187) and Berzelianite $Cu_{2-x}Se$ (JCPDF 71-0044) for samples grown at T_{Iodine}= 60°C, and to stoichiometric Cu_2Se (JCPDF 37-1187) for samples grown at 70°C. However, Cu_2Se (030) and $MoSe_2$ (002) peaks may overlap around $2\theta \sim 13.5°$, and the appearance of thin type II domains of $MoSe_2$ thus cannot be excluded in those samples grown under moderate T_{Iodine}, that may account for the broadening of the corresponding Cu_2Se (030) signal recorded in comparison to the sample annealed at high T_{Iodine}. This interpretation is further supported by the formation of metallic Cu in samples annealed at high T_{Iodine}, which may prevent the formation of $MoSe_2$ once the substrate surface is covered. The sharp peak at 13.5° of the sample at T_{Iodine}= 70°C is confidently attributed to the Cu_2Se (030) reflection.

3.3.2.3 Substrate conditioning

It has been found that the reproducibility of the $MoSe_2$ layer thickness from different CVD processes carried out following identical recipes depends sensitively on the conditioning of the Mo substrates. In order to perform comparative studies on the evolution of the $MoSe_2$ formation it is thus mandatory to start from Mo coatings of the glass substrates that have been prepared from the same sputtering runs. Substrate oxidation and aging may alter the availability of Na at the substrate surface and/or the oxidation state of the uppermost Mo atomic layers, resulting in non-reproducible selenisation processes when comparing samples processed from different sputtering batches.

With this premise, Mo-coated glass substrates from the same sputtering processes were processed under Ga_xCl_y/H_2Se, as stated in the previous section. Figure 45 shows XRD diffractograms obtained from two different samples after annealing times of 1 and 4 hours, with $MoSe_2$ thickness of 11 nm and 39 nm, as estimated from XRF analysis. As a comparison, the final thickness of the chalcogenide layer found on those substrates also annealed under Ga_xCl_y/H_2Se included in Figure 44 were 85 nm (45 min. annealed sample) and 93 nm (4 h. annealed sample). No correlation between the $MoSe_2$ thickness and the processing time under the given conditions of these four samples can thus be inferred from the analysis, as long as the substrates used for these processes were stored in laboratory ambient during different periods of time.

Focusing on the samples shown in Figure 45, a nearly linear relationship is found between the processing time on the sample and the corresponding $MoSe_2$ layer thickness, leading to a growth rate of ~10 nm/h. Additionally, it can be concluded from the intensity evolution of the different peaks, that the formation of type II $MoSe_2$ takes place during the early stages of the film growth, with (002) reflections dominating the diffractogram of the sample annealed during one hour. No further development of domains with type II orientation takes place when increasing the processing time, as the (002) peak intensity remains unaltered after 4 hours processing. However, those reflections characteristic of type I orientation and mixed character develop with longer processing times, accounting for the total layer thickness increase. These results are in agreement with TEM pictures, like that shown in Figure 42, where type I orientation is found in nearly 95 % of the total $MoSe_2$ layer thickness. A growth model of the $MoSe_2$ developed during the growth of CGSe in the CVD set-up can be proposed based on these observations, where the early stage of Mo selenisation results in type II $MoSe_2$. The total thickness after this stage is limited to 15-25 nm, according to TEM cross-sections. Such limited growth of type II thin films of layered metal chalcogenides is commonly found[157], and is likely related to the limited diffusion of chemical species across van der Waals planes. Domains of type II orientation are thus constrained to a relatively narrow thickness. Further growth of $MoSe_2$ takes place undergoing a change from type II to type I orientation, which is recorded by the appearance of XRD peaks related to type I and mixed character reflections for longer processing times.

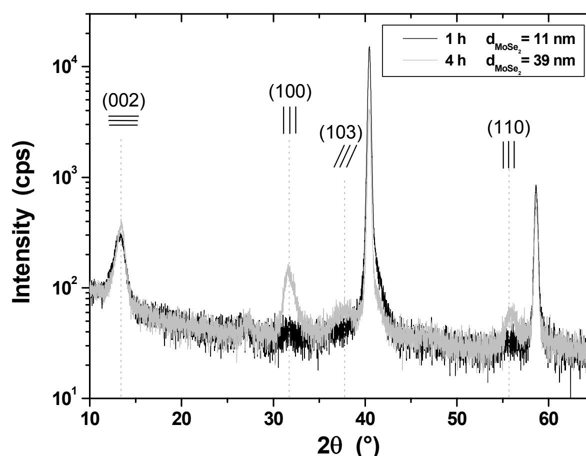

Figure 45. XRD diffractogram of Mo-coated SLG substrates subjected to annealing processes under Ga_xCl_y/H_2Se gases at $T_{substrate}$= 500°C during 1 and 4 hours. Dominant peaks from $MoSe_2$ are labelled, with the related basal plane orientation indicated.

No satisfactory explanation has been found for the bending process governing the smooth transition from type II to type I orientation and the further inwards growth of $MoSe_2$ into the Mo film. The coexistence of type I and type II domains in thin films of layered transition metal dichalcogenides has been, however, reported in the literature, as a result of branching processes with an abrupt change in the orientation of the basal planes[158]. Such branching mechanisms result in inverted structures to those found in this study, i.e. type II orientation usually takes place first at the bottom of the layer, with type I branches growing upwards from it[158,159]. Branching points are randomly distributed in the layer bulk, leading in certain cases to complex dendritic structures of the layered compound. Computer simulations were reported[158] for the modelling of the branching mechanisms, demonstrating that a congruent lattice disposition of crystallite domains of both parallel and perpendicular orientations is required in order to induce such a growth change. No references to other chemical species involved in the branching process were included in these studies. However, Barreau *et al.*[160] proposed a model to account for the experimental findings on the influence of Na in the texturisation of MoS_2 films, based on the formation of metastable tetra-thiomolybdate compounds that control the orientation of the developing layered compound, which was generalised to the case of the presence of Ni and K additives. The difficulty of confirming *in situ* the formation of such metastable compounds during sample processing hinders however the validity of the model for the case under study. Nevertheless, the presence of metallic species (specially Ga) during the CGSe growth could presumably have similar effects to those reported for Na, Ni and K, a hypothesis that would attribute an active role to the cation species in the gas phase in relation to the progressive orientation change found in $MoSe_2$.

The presence of $MoSe_2$ as an intermediate layer at the back contact of thin-film solar cells based on chalcopyrite absorbers has also been reported by some authors. T. Wada and co-workers[161] identified the layered compound from SIMS depth profiles of $Cu(In,Ga)Se_2$ absorbers grown on Mo-coated glass substrates by co-evaporation. Cross-sectional TEM analysis combined with micro-EDX measurements revealed the morphology and composition of the interfacial layer[162,163]. Detailed studies carried out

subsequently by Nishiwaki *et al.* [164] on the formation of $MoSe_2$ under modified growth conditions from those used in a conventional three-stage co-evaporation process for high efficiency Cu(In,Ga)Se_2 devices[165] led the authors to conclude that both the thickness and the relative orientation of the $MoSe_2$, as determined from TEM and XRD analysis, show a clear dependence on the temperature and gas composition during the absorber film growth. In particular, Cu-rich conditions were reported to inhibit the formation of the layered compound, with typical final layer thickness below 10 nm, whereas (In-Ga)-rich stages seemed to correspond to the fastest growth rate of the $MoSe_2$ layer at normal processing temperatures around 550°C, leading to layer thickness of 150 nm. Additionally, the presence of Ga and In in the gas phase was found necessary in order to achieve type I orientation, whereas either direct selenisation of the Mo substrate or Cu-rich conditions in the gas phase led systematically to type II orientation. A summary of these results is given in Table 3.

Table 4. Summary of results by Nishiwaki et al.[164] on the formation of $MoSe_2$ during the growth of Cu(In,Ga)Se_2 (CIGSe) under modified conditions during the first and second stages and after completion of the standard three-stage process developed at NREL[165]. Layer thickness, orientation type and XRD reflections of the $MoSe_2$ are included.

1st stage	T (°C)	2nd stage	T (°C)	$MoSe_2$	
Se	550			10 nm (II)	XRD (002)
Cu+Se	550			< 10 nm (II)	XRD (002)
Cu+In+Ga+Se (Cu-rich CIGSe)	550			<<10 nm (II)	XRD (002)
In+Ga+Se	350	Se	550	100 nm (I)	XRD (100), (110)
In+Ga+Se	350			-	-
In+Ga+Se	350	Cu+Se	550	(I)	XRD (100), (110)
CIGSe (device-grade)				*150 nm (I)*	

These results are in general agreement to those found in the CVD growth of CGSe films, except in the unique feature of the progressive transition from type I to type II across the $MoSe_2$ layer when approaching the CGSe interface. It should also be mentioned that under standard CVD conditions described above, the provision of Group III element into the gas phase in the form of the gaseous halide Ga_xCl_y is accompanied with excess H_2Se. It is thus not possible to distinguish separately the effects on Mo selenisation related to the presence or absence of Ga_xCl_y mixed with the selenising agent H_2Se.

As a closing remark of this section, it is perhaps worth mentioning that the growth of $MoSe_2$ thin films, by means of a variety of techniques, like electrodeposition[166], d.c. diode sputtering[167], and selenisation of Mo substrates[168,169], has been a matter of study of different research groups, as this compound shows itself convenient properties for the implementation of photovoltaic devices[170]. The reasons behind are on the one hand a high absorption coefficient[150,171], similar to that shown by Cu-containing chalcopyrites, in the range of 10^5 cm^{-1}, and on the other hand the nearly optimal value of the energy band gap for the absorption of the sunlight (between 1.1 and 2.0 eV) shown by this and related layered compounds, like MoS_2 and WS_2.

3.4 Improvements in film deposition

As stated in the preceding sections, the quality of the active absorber layer of thin-film solar cells processed from CVD-grown CGSe depends sensitively on the deposition conditions established in the reactor during the growth. Severe limitations to the growth of high-quality material have been identified, which are summarised in the following statements:

- The requirement of slightly Ga-rich overall compositions in order to obtain device-grade quality of the CGSe absorber films is difficult to combine with a film thickness above 1.5 μm for optimal carrier collection and a convenient morphology characterised by large columnar grains and a reduced number of grain boundaries.
- Such convenient structural properties are nevertheless accessible when moving from Ga-rich to stoichiometric or slightly Cu-rich compositions, but at the expense of inducing detrimental effects on the electronic quality of the CGSe film.
- The appearance of copper selenide secondary phases has a negative influence on device performance, due to their nearly-metallic character and associated effects in the subsequent device processing. The role of $MoSe_2$ in the mediation of the rear contact will be addressed in Chapter 4.

The introduction of improvements in the open-tube CVD-based deposition process of CGSe thin films for PV applications, based on the analysis and identification of limiting factors stated in the preceding sections, constitutes the core of the present work. Three approaches will be presented targeting high-quality and high-PV yield of CVD-grown CGSe films and related devices:

- implementation of sequential deposition processes,
- use of metal precursors,
- and the lift-off procedure.

The first two approaches are presented in the following sections. The corresponding device characterisation will be presented in Chapter 4 in a comparative study of single- vs. sequential- and metal-precursor-based deposition processes. The lift-off technique will be presented in Chapter 5.

3.4.1 The two-stage process

The characteristic composition-dependence of the growth rate shown by Cu-containing chalcopyrites, together with the role of quasi-liquid species controlling the incorporation of material during the film growth, have led to the implementation of sequential deposition processes in a variety of growth technologies for these compounds. A pioneer work was reported by Mickelsen[172], that came to be known as the 'Boeing' or 'bilayer' PVD process, consisting in the change of evaporation rates of elements of Groups I and III offered to the substrate during the deposition process. This approach, with minor modifications depending on the growth system employed, is commonly used for the growth of chalcopyrite films in a large number of research centres, and has been recently introduced in industrial production[119]. Cu-rich compositions promote a rapid

film growth in the early stage, whose electronic properties are optimised afterwards by a Group-III enrichment stage. Further refinements on the bilayer process have been subsequently introduced, with special mention to the 'three-stage-process' reported by the group at NREL[165] for $Cu(In,Ga)Se_2$, holding the absolute record of PV efficiency under AM1.5G standard conditions of a polycrystalline thin-film solar cell[7].

The implementation of sequential deposition processes based on changes of the gaseous composition during a single run is not possible in standard CVD systems, as long as we deal with closed systems. However, the flexibility of the open-tube two-sources CVD system allows varying the composition of the gas flow on the substrate side by adjusting the gaseous flows sweeping the source boats during the deposition process. This unique feature in a system based on chemical vapour transport opens the possibility of combining highly flexible operation conditions with moderate processing temperatures, yielding in the case of CGSe device-grade material comparable to that obtained from standard co-evaporation.

Following the 'bilayer' approach, a two-stage process has been adapted for the CVD system. The first stage of the sequential process is carried out during 3-4 hours at a substrate temperature of 500°C. Both lines of Cu_2Se and Ga_2Se_3 are open and swept by transport gases I_2/HI and HCl, respectively, producing nearly stoichiometric CGSe samples with thickness between 1.5 and 3 μm and crystallites of the same dimensions. The second stage consists of Ga_2Se_3 transport with HCl during typically 20 minutes at a substrate temperature of 530°C, which ensures a final Ga-rich overall composition ([Ga]/[Cu](s)~1.1) desired for optimum cell performance. Standard parameters used for the growth of device-grade CGSe films are given in Appendix I. The two-stage approach overcomes the difficulties related to small crystallite sizes and film thickness shown by Ga-rich single-stage based films, providing a convenient path for growing slightly Ga-rich films with the preferred morphology of stoichiometric layers. Furthermore, optical measurements have demonstrated a significant reduction of sub-band gap absorption of nearly one order of magnitude, as well as related deep luminescence[128] in samples grown by two-stage processes, both aspects related to a high density of defect states in the absorber band gap, compared to those processed from single-stage runs. The direct influence of the sequential deposition process on the electronic quality of the absorber is recorded in the improved PV performance of related devices, as will be discussed in Chapter 4.

Cross-sectional studies on complete devices based on two-stage grown absorbers have been carried out in parallel to those reported on Cu-rich samples shown in the previous section. In particular, the chemical bath for the CdS buffer layer deposition was prepared following the same recipe given in Chapter 1. Figure 46 shows the TEM cross-section presented in Figure 42 (from a two-stage sample, although not mentioned there) and the corresponding EDX mappings of Cu-, Ga-, Se-, Mo-, Zn-, Cd-, and S-K signals. Contrarily to the case of Cu-rich compositions, two-stage samples consist of single phase CGSe as inferred from the even distribution of Cu, Ga and Se, in agreement with the phase diagram of Figure 28 and the experimental observation of no Ga_2Se_3 phase formation even for highly Ga-rich compositions. $MoSe_2$ is well resolved from the Se and Mo mappings, with no differences found in this respect between single- and two-stage based samples. A remarkable difference compared to the case of Cu-rich compositions is the formation of a closed and homogeneous CdS buffer layer, as revealed by the corresponding mappings of Cd and S signals (some damage from the sample preparation can be recognised on the left part of the buffer/window system in

the TEM picture and the corresponding mappings). The S K-line overlaps the Mo L-line, as indicated in the corresponding EDX mapping in Figure 46. The effects of the buffer layer on the interface band alignment will be further discussed on the basis of KPFM studies.

The presence of single phase CGSe in samples grown by two-stage processes has been checked by realising the second stage of the sequential process on Cu-rich samples grown in single-stage processes. Figure 47 compares XRD diffractograms of the same sample, grown under Cu-excess ([Ga]/[Cu](s)=0.97, from EDX) and including copper selenide segregations, before and after processing the second stage as described above during 20 minutes ([Ga]/[Cu](s)=1.12, from EDX). Peaks related to the secondary phase disappear after completion of the Group-III enrichment stage. It is concluded that the second stage acts effectively as a refining step, able to dissolve Cu-rich segregations into the chalcopyrite matrix, at the expense of increasing the overall [Ga]/[Cu] ratio.

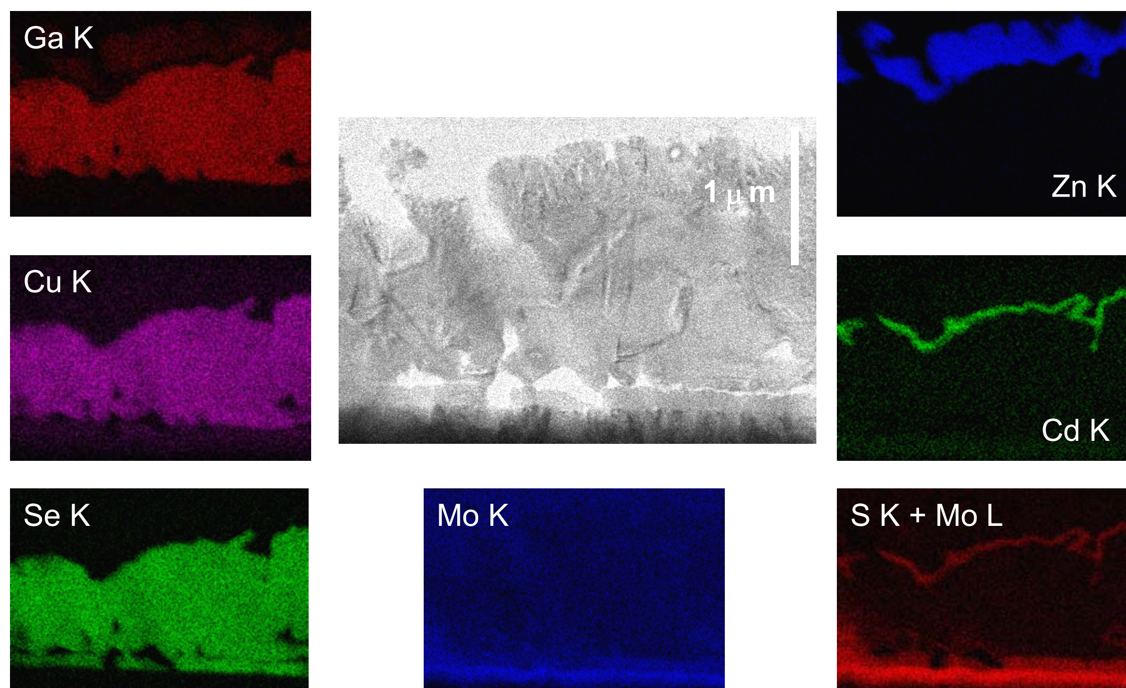

Figure 46. TEM cross-section shown in Figure 42 (middle up) of a two-stage-based CGSe solar cell and corresponding EDX mappings of elements forming the Mo substrate, the CGSe absorber, the CdS buffer and ZnO window layers.

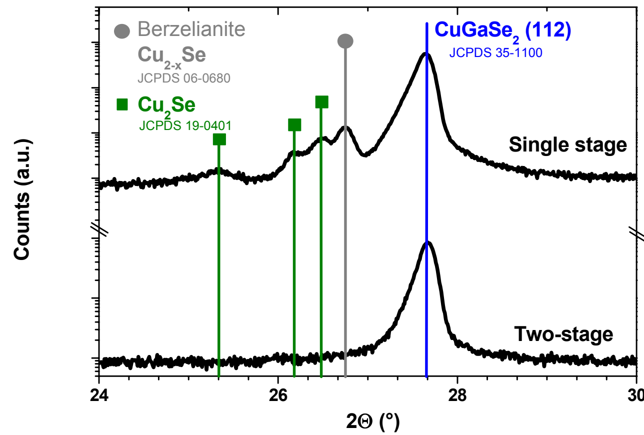

Figure 47. XRD patterns of a CGSe sample after single- ([Ga]/[Cu](s)=0.97, from EDX) and two-stage ([Ga]/[Cu](s)=1.12, from EDX) processing. Copper selenide phases are removed after the Group-III enrichment stage.

Cross-sections of two-stage-based devices were processed for KPFM analysis, following the same procedure as for the Cu-rich single-stage samples shown in Section 3.3.1. Figure 48 (a) and (b) show the topography and work function scans measured simultaneously on one of these samples, after the completion of the sputter-cleaning process described before, consisting in 1 hour annealing at 110°C and 15 minutes of sputter-cleaning with Ar^+ at 500 eV and 45° incident angle. The topography image shows some contrast between the layers that helps delimiting different work function regions on the corresponding picture. A remarkable granular structure is visible on the CGSe and substrate layers, which is partly attributed to the persistence of adsorbates. Figure 48 (c) shows the work function scan at the same position under illumination (λ=442 nm, p~60 mW). The work function of CGSe and $MoSe_2$ increases slightly under illumination, in agreement with a reduction of the surface band bending expected from p-type semiconductors explained before. Nearly flat band conditions might be assumed to prevail under illumination, following the discussion in Section 3.3.1, although we will refer back to this point at the end of this section. Under illumination, an average value of the CGSe work function of 4.96±0.03 eV is obtained.

Despite of some degree of surface modification, as pointed out before, it should be stressed that average work function values measured in Figure 48 (b) and (c) are nevertheless in the range of expected values, as shown in Table 3, when comparing to measurements on as-grown CGSe films carried out on samples transferred in inert gas atmosphere. The evolution of work function values with longer sputter-cleaning times has been recorded in the mappings shown in Figure 49 and 50. These figures show the topography and corresponding work function values in the dark at different positions after 30 and 60 minutes sputtering and 2 hours annealing at 110°C. Single grains in the absorber layer can be seen in the topography images, presumably due to a preferential sputtering at grain boundaries. A deeper trench can be seen in Figure 50 between the absorber and the window layers, also related to an effective sputtering of the CdS buffer layer during the cleaning process. Line-scans from the topography and work function images are included and shown in Figure 51.

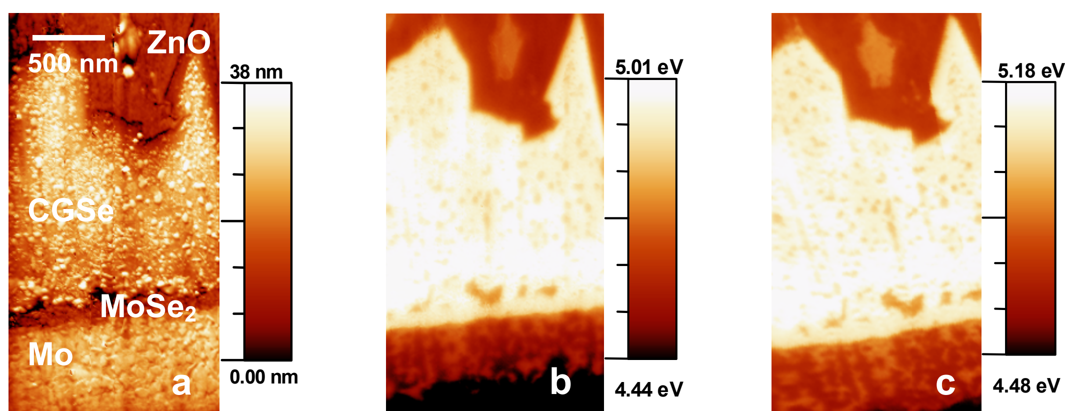

Figure 48. KPFM cross-section images of a CVD-CGSe-based solar cell from a two-stage process, after 1 hour annealing and 15 minutes Ar^+ sputtering at 500 eV and 45° incident angle. **(a)** topography, **(b)** work function in the darkness, and **(c)** work function under super-band gap illumination (λ=442 nm, p~60 mW).

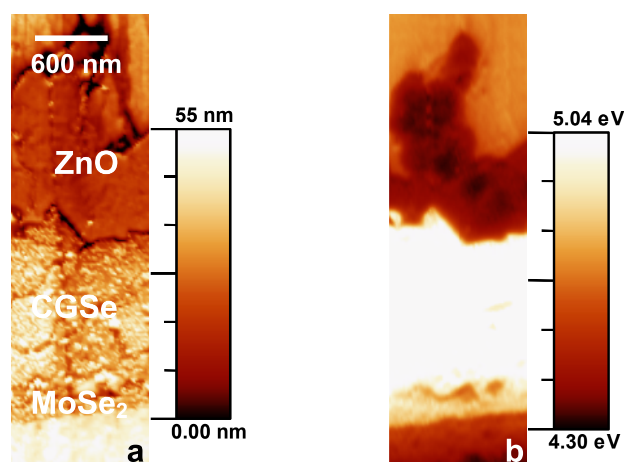

Figure 49. KPFM cross-section images of a CVD-CGSe based solar cell from a two-stage process, after 1 hour annealing and 30 minutes Ar^+ sputtering at 500 eV and 45° incident angle. **(a)** topography, **(b)** work function in the darkness.

A remarkable surface roughness is inferred from the topography line-scan shown in Figure 51, mainly constrained within the absorber layer. This result suggest a selective surface sputtering, probably leading to the formation of metallic Ga-clusters, in agreement with previous reports from Otte *et al.*[138] on sputter-cleaning procedures on $CuInSe_2$ and $CuGaSe_2$ chalcopyrites. This result remarks the tight trade-off between sputter cleaning and surface modification, already pointed out in Section 3.3.1. From our results, short sputtering cycles of 5 to 10 minutes using moderate energies of 500 eV, followed by annealing steps, are recommended for samples which have been exposed to air, though close monitoring of the evolution of recorded values is mandatory for certifying the effectiveness of the procedure.

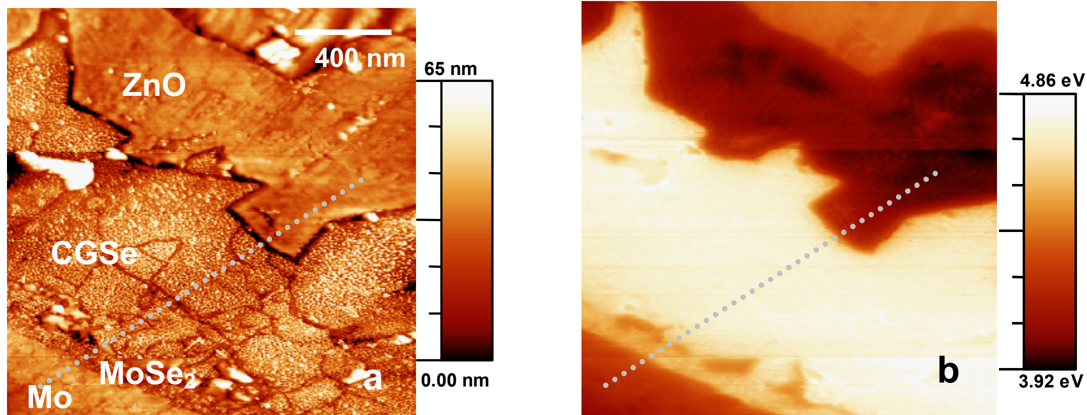

Figure 50. KPFM cross-section images of a CVD-CGSe based solar cell from a two-stage process, after 1 hour annealing and 60 minutes Ar^+ sputtering at 500 eV and 45° incident angle, **(a)** topography, **(b)** work function in the darkness.

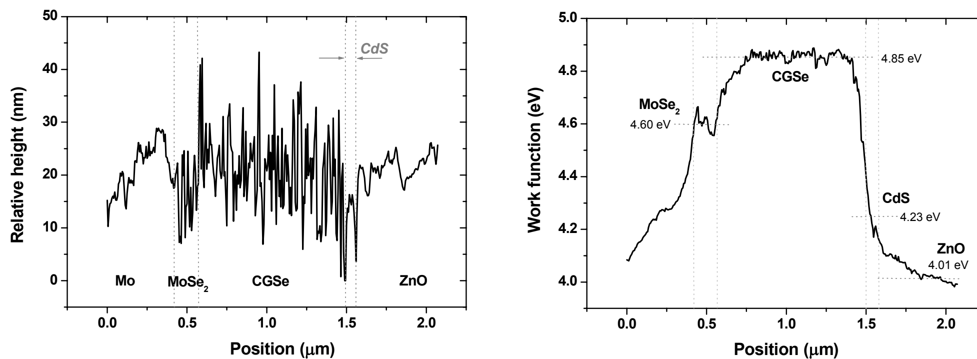

Figure 51. Line-scans from Figure 50, topography **(left)** and work function **(right)**. Significant roughness is found within the limits of the absorber layer, attributed to cluster formation resulting from the sputtering cleaning process. A minimum built-in potential V_{bi} >840 mV (excluding SPV) at the p-n junction is inferred from the change in work function between the CGSe absorber and the ZnO window layer.

Comparing the work function line-scans of Figure 51 and 37, as well as the work function mappings of Figure 48-50 to those of Figure 34-35, a clear difference is found regarding the influence of the buffer layer on the band alignment of devices based on Cu-rich and Ga-rich materials (the formers, not being subjected to wet etching treatments). In contrast to the potential barrier of nearly 200 meV found in Cu-rich based devices, a favourable downwards band bending is inferred from the work function profile depicted in Figure 51, when moving from the p-type absorber layer into the n-type window layer, following the path of minority carriers being injected by the p-n junction under standard operation conditions. This result supports the attribution of the potential barrier found in Cu-rich based devices to the presence of an extraneous Cu-S layer replacing the expected CdS buffer, as result of the $Cu_{2-x}Se$ surface segregation during the deposition process of CGSe under Cu-rich conditions. Additionally, a slightly higher built-in potential (up to ~150 mV) of the p-n junction in the two-stage-

based device is inferred from the relative potential drop associated to the change in work function (Φ/q), when comparing to the case of Cu-rich single-stage devices (see Figure 37 and 37). This observation is agreement with the experimental fact that higher open-circuit voltages are accessible from Ga-rich compositions of CGSe absorbers when processing devices[127]. We will refer to the influence of these values on the obtainable open-circuit voltages of solar cells processed from single and two-stage absorbers in Chapter 4.

Figure 52 summarises the evolution of the average work function values obtained at different positions, as a function of the sputtering/annealing steps to which the samples shown in Figure 48 to 50 were subjected. Open symbols represent values under illumination. Presuming flat band conditions, the average work function value of the CGSe absorber film after 15 minutes sputtering is 4.96±0.03 eV, which combined with electron affinity values χ~4.1 eV from the literature[173] and a band gap energy of ~1.65 eV, as discussed in Chapter 4, results in the Fermi level lying at ~0.79±0.03 eV from the valence band maximum, in agreement with previous reports based on XPS studies[174] on non-treated and slightly Ga-rich CGSe surfaces. This value E_F-E_V~0.8 eV will be found again on the CGSe top surface of Ga-rich (two-stage) samples from UPS studies in Chapter 4. For highly doped ZnO, the work function lies at 4.26±0.03 eV, in agreement with the results from Moormann *et al.*[175]. A maximum value of the work function Φ=5.05±0.02 eV is obtained for CGSe after 30 minutes sputtering, likely corresponding to the optimal situation between adsorbate-cleaning and surface modification induced by the sputter/annealing steps. Longer sputtering times result in an overall reduction of all work function values, which is attributed to a severe electronic modification and clustering effects on non-stoichiometric surfaces.

Despite this effect, the absorber layer maintains a nearly constant work function value under super-band gap illumination, which may indicate Fermi level pinning in near mid-gap regions from the numerical estimations above. For this reason, it is stressed that the measured surface photovoltage, though effectively bringing the sample towards flat band conditions by reducing the surface band bending, may not lead to strict fulfilment of that statement, limiting the validity of the assumptions which led to the results shown in Eq. 115. As stated in that paragraph, the difficulty of splitting the 2-dimensional band bending in two different contributions of the potential drop, one related to the p-n junction and the other related to the p-vacuum surface, lies on the weak assumption of the elimination of the second contribution with sufficiently intense illumination. Only under low surface recombination velocities, in clear opposition, e.g. to Fermi level pinning conditions, may this be the case. So-calculated values of the net doping concentration must therefore be considered only as a minimum value, subjected to reanalysis by other means of electronic characterisation, as shown in the next chapter.

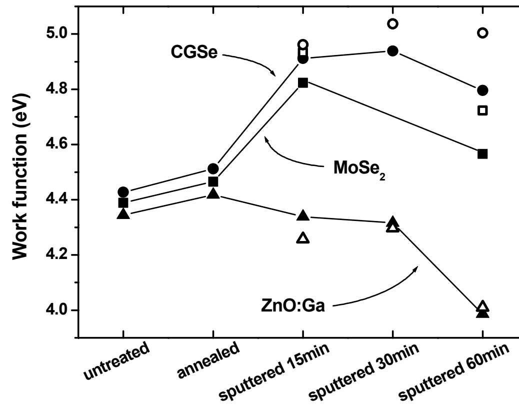

Figure 52. Work function values of the different layers making up the two-stage-based CGSe solar cell studied in the previous cross-sections, after different stages in the cleaning process. Solid symbols denote values measured in darkness. Open symbols denote the values under super-band gap illumination (λ=442 nm, p~60 mW).

3.4.2 Metal precursors

In the case of Cu-based chalcopyrites, metal precursors consisting of Cu or In/Ga layers are routinely used in rapid thermal processing of $CuInS_2$ and $Cu(In,Ga)Se_2$. This technique simplifies the growth process, as part of the elements can be easily deposited, e.g. by sputtering or evaporation. Additionally, the growth rate of the layer can be enhanced due to the rapid formation of quasi-liquid species, like $Cu_{2-x}Se$, according to the model proposed by Klenk[54], which can effectively drive the subsequent growth reaction. Furthermore, metal precursors may protect the metallic rear contact against its eventual sulfurisation/selenisation, a process which can have detrimental effects on both the adhesion and performance of the absorber film in solar cells.

In this work, the use of Cu-precursors has been studied as a potential alternative to the use of two binary sources for CVD applications. Cu-layers of 200 and 500 nm thickness have been sputtered on Mo-coated soda-lime glass and used as substrates for CGSe deposition. Different recipes have been used, comprising either full two-stage processing or single-stage processing with one source (Ga_2Se_3). The latter approach has additional technological interest, as it has been adapted for its application in the recently developed close-spaced CCSVT set-up[176]

3.4.2.1 Two-stage processing of Cu-precursors

A remarkable increase of up to 70 % in the CGSe growth rate has been found in Cu-precursor substrates, compared to standard Mo-coated substrates from the same run. This enhanced growth rate permits to downscale the deposition process to shorter times, as a film thickness above 4 μm does not further improve the PV performance of final devices.

The crystallinity and composition of the films have been checked by means of XRD, XRF and EDX, confirming the presence of single phase CGSe in those samples fully processed with a sequential deposition recipe (see Appendix I).

Figure 53 shows a SEM cross-section of a thin-film solar cell based on CVD-CGSe grown on a 200 nm thick Cu-precursor. A typical crystallite morphology corresponding to samples grown under Cu-rich conditions can be recognised, with polyhedral crystallites of dimensions above 2 μm, comparable to those found in the top view of Figure 26 (right) from slightly Cu-rich single-stage samples. A complete substrate coverage, apart from characteristic voids, is achieved, contrarily to the case found on Cu-rich single-stage samples, due presumably to the different wetting process and reaction kinetics involved in the presence of the Cu-precursor. These aspects will be discussed in the next section. The analysis of the PV performance of devices based on Cu-precursors is deferred until chapter 4.

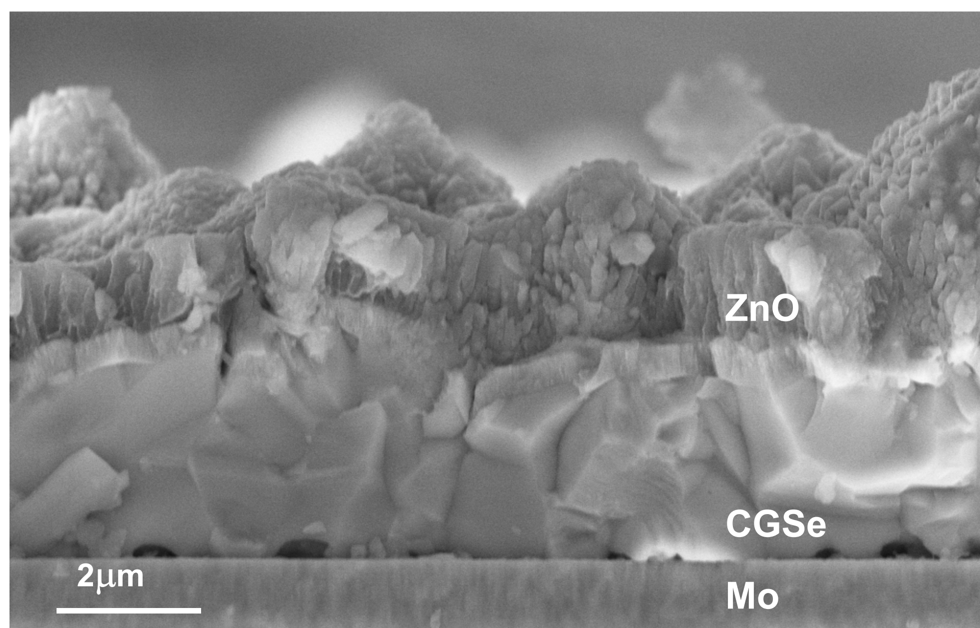

Figure 53. SEM cross-section of a CVD-CGSe based thin-film solar cell. The absorber was deposited following a two-stage process on a Cu-precursor of 200 nm thickness. Large-grained films and a complete substrate coverage characterise the growth of these samples.

3.4.2.2 Single stage processing of Cu-precursors and the reaction process

A second and simpler approach to the use of Cu-precursors in the open-tube CVD system consists in the realisation of single stage processing using solely the Ga_2Se_3 line. This approach has been used for the study of the reaction kinetics on the substrate side and has been monitored in a series of interrupted processes after different processing times.

Figure 54 shows a SEM picture and the corresponding EDX-mappings of a face-to-face cross-section prepared from a 500 nm thick Cu-precursor layer annealed during 1 hour under Ga_xCl_y and H_2Se in the CVD system. Thicker Cu-precursors are used in this approach, as no additional Cu-supply is provided during the process. The presence of $Cu_{2-x}Se$ secondary phases can be inferred from the uneven distribution of Cu and Ga signals, as in single stage Cu-rich samples in Figure 31. These phases are distributed as a thin layer close to the rear interface, as well as in large domains in the film bulk, indicated by arrows in the Cu- and Ga-EDX mappings.

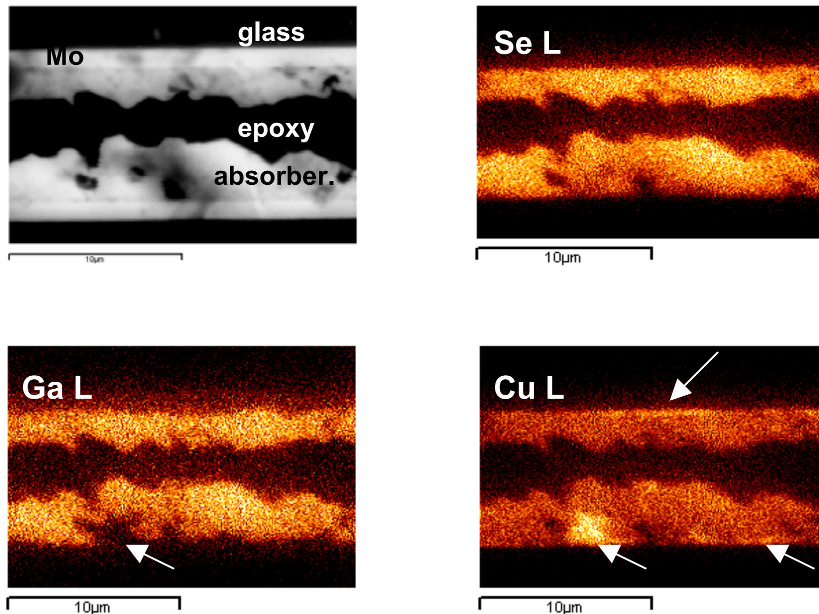

Figure 54. SEM cross-section (upper left) and corresponding EDX-mappings of Cu, Ga and Se L-lines, of a face-to-face preparation from a 500 nm Cu precursor on Mo-coated SLG substrate, subjected to 60 minutes processing under Ga_xCl_y/H_2Se atmosphere in the CVD system (T_{sub}= 500°C). Arrows in the Cu and Ga maps indicate locations of Cu-rich phases.

Cross-sections from the same sample shown in Figure 54 were prepared for TEM analysis, an example of which is shown in Figure 55 left. A double structure in the absorber film is visible, with a dark-contrast region close to the substrate interface, showing a characteristic fracture plane, and a brighter region up to the top surface. A series of EDX point measurements along the sample thickness, shown as a line-scan in Figure 55 right, confirms the Cu-rich composition of the bottom layer, with a Cu content of nearly 70 at%. The presence of a Cu-rich phase in the absorber close to the interface with the Mo substrate can also be inferred from the Cu-L EDX map of Figure 54. Compositions corresponding to nearly stoichiometric CGSe are found across the bright area, except in certain clusters of ~200 nm diameter visible in the TEM picture, showing compositions in agreement with $Cu_{2-x}Se$.

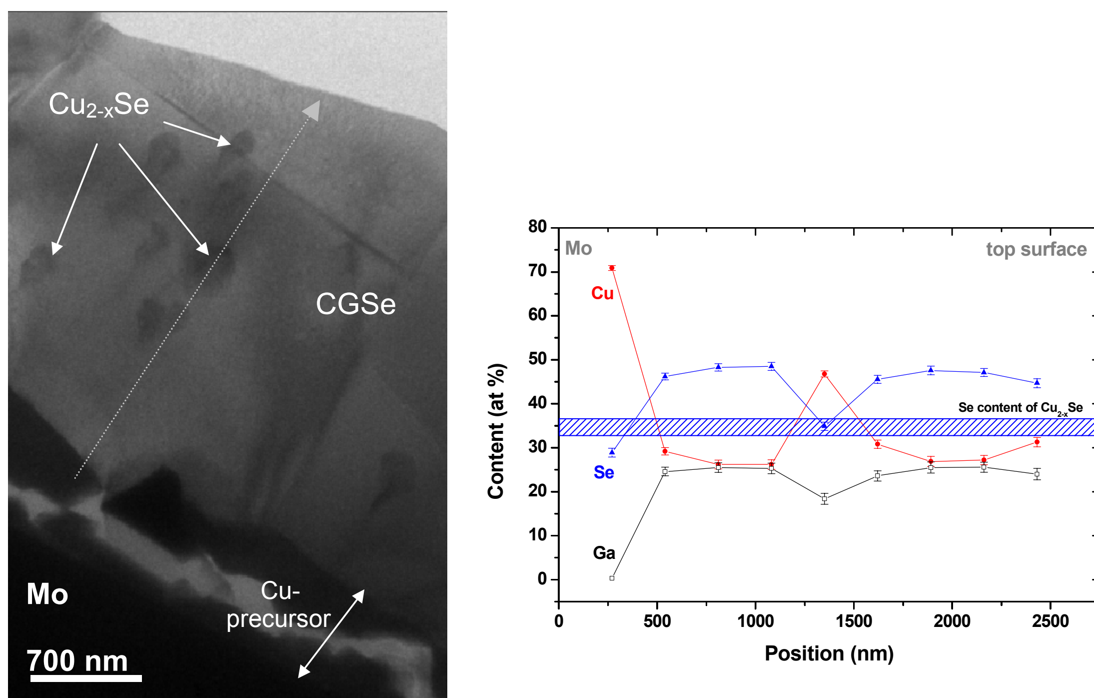

Figure 55. (Left) TEM cross section of a 500 nm thick Cu-precursor processed under Ga_xCl_y and H_2Se during 1 hour. CGSe forms the upper bright contrast phase, whereas copper selenides are found embedded in the absorber film. Not fully selenised Cu remains at the rear contact (dark contrast) showing a fracture plane filled with epoxy. **(Right)** EDX point measurements corresponding to the dotted line on the left figure.

It is thus concluded that the 500 nm thick Cu-precursor is not fully selenised after 1 hour processing, though a film thickness above 2 μm is already recorded. Cu consumption from the precursor leading to CGSe formation out from the precursor top surface is considerably more effective than the incorporation of elements into it. This is due on the one hand to the high mobility of Cu ions in the CGSe matrix[177], and on the other hand to the formation of copper selenides in the uppermost part of the Cu precursor during the first stages of film growth.

Intrusions of $MoSe_2$ 20-60 nm long are also found at the interface between the Mo substrate and the Cu-rich layer, showing a preferential type-II orientation. An example is shown in Figure 56. Certain regions of the characteristic saw-teeth fracture plane found in the Cu-rich bottom layer correspond to the $MoSe_2$ interface, a fact that could be directly attributed to the preferential type-II orientation and the easy cleavage associated to it.

Figure 57 shows a second cross-section prepared from the same sample as the one shown in Figure 55, after processing a second annealing step of 60 minutes on it. A similar fracture plane is visible, entirely corresponding in this case to the absorber/$MoSe_2$ interface. A line-scan performed over a number of EDX point measurements is also shown in Figure 57, revealing the presence of single phase CGSe throughout the entire film thickness. A slightly Ga-rich composition is indeed found after 120 minutes processing.

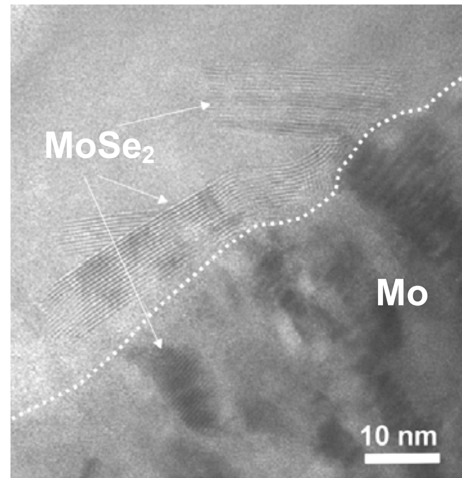

Figure 56. HRTEM picture of the CGSe/$MoSe_2$ interface of a 500 nm thick Cu-precursor processed under Ga_xCl_y and H_2Se during 1 hour, revealing the presence of domains of type-II $MoSe_2$.

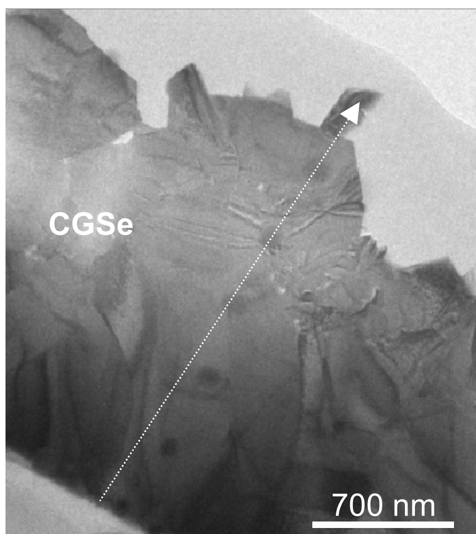

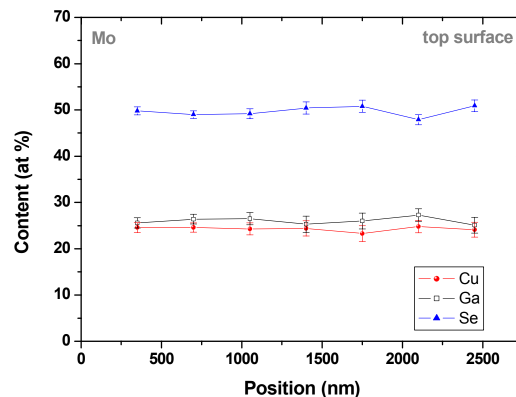

Figure 57. (Left) TEM cross section of a 500 nm thick Cu-precursor processed under Ga_xCl_y and H_2Se during 2 hours. The film peeled off from the substrate (not visible, on the lower left corner) at the $MoSe_2$/CGSe interface. **(Right)** EDX point measurements corresponding to the dotted line on the left figure. Single phase CGSe is found throughout the entire film thickness.

$MoSe_2$ is found to develop further with longer processing times, as can be seen in Figure 58, showing the CGSe/Mo interface of the sample annealed during 2 hours under Ga_xCl_y and H_2Se. Thicker domains of $MoSe_2$ are present at the absorber/substrate interface. Remarkably, the characteristic transition from type-II to type-I orientation reported in Section 3.3.2 is again found in certain locations of the cross-section, as indicated in Figure 58. The transition takes place coinciding with a significant increase of Se-content at the rear surface of the absorber layer, from nearly 33 at% that would

correspond to a fully selenised Cu-precursor (stoichiometric Cu_2Se, not achieved in Figure 55), to about 50 at% corresponding to CGSe, and a parallel increase in the Ga concentration, from residual amounts up to nearly 25 at% in final CGSe. From these results, and those presented in Section 3.3.2, it follows that the characteristic structural rearrangement found in the $MoSe_2$ layer during CVD processing requires the concurrent presence of Ga and Se species on the Mo surface, which is in turn a singular feature of the open-tube CVD system based on two sources.

From the results of this section on the use of Cu-precursors subjected to annealing in Ga_xCl_y and H_2Se it is concluded that the Cu-precursor controls the growth of the CGSe film in two stages. First, by a progressive selenisation and release of material, resulting in an outwards Cu-rich film development on the one hand, and a reduced Mo selenisation on the other hand. And second, by the transformation of the slightly Cu-rich material into Ga-rich CGSe as the processing time increases, with an effective enhancement of the $MoSe_2$ growth and the activation of the transition from type II to type I of the chalcogenide layer.

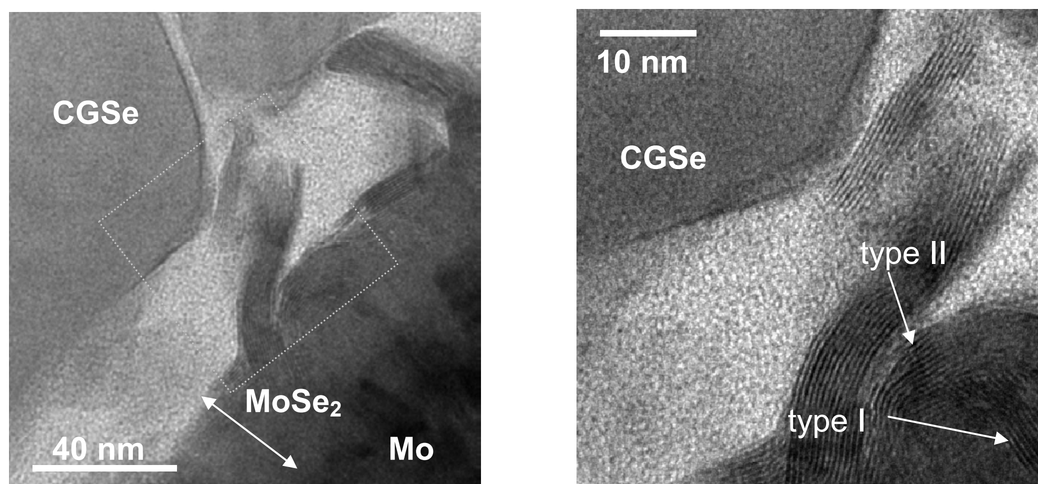

Figure 58. **(Left)** HRTEM picture of the CGSe/$MoSe_2$ interface of a 500 nm thick Cu-precursor processed under Ga_xCl_y and H_2Se during 2 hours. $MoSe_2$ developed further during the second hour of processing, compared to Figure 56. **(Right)** Enlarged picture of the area enclosed on the left image, showing both orientations of the $MoSe_2$ layer.

3.5 Chapter summary

The basics of the open-tube CVD processing of CGSe thin films have been reviewed, with particular attention to those aspects of the growth process related to the quality of the absorber film for PV applications.

It has been found that a number of potential limitations may affect the growth of CGSe films in single-stage-based processes. Concretely, the exponential dependence of the film growth rate and the related film morphology on the composition of the gaseous species participating in the chemical transport, do not facilitate the growth of device-quality films, which should be accomplished by the simultaneous concurrence of a preferable film morphology, typical of nearly stoichiometric films, together with improved electronic properties, characteristic of slightly Ga-rich compositions.

In relation to composition-dependent issues, the formation of secondary phases during the growth of CGSe films has been investigated, performing microstructural analysis on those extraneous phases found in the samples in order to determine their influence on subsequent device processing and performance. Copper selenides of two types, namely stoichiometric Cu_2Se and non-stoichiometric $Cu_{2-x}Se$, related to Cu-rich conditions during the growth of CGSe films, have been found to form entire crystallites, surface layers around CGSe crystallites and clusters embedded in the CGSe matrix. They show detrimental electronic properties for PV applications, due to the nearly metallic character associated, and their presence must be avoided in final layers for subsequent device processing. In this respect, the requirement and efficacy of surface etching treatments prior to the buffer deposition on Cu-rich polycrystalline samples has been discussed, with special reference to the formation of a related Cu-S layer during CBD processing of the buffer layer. Copper selenide phases and improper buffer layers result in unfavourable band line-ups for the diffusion of minority carriers, including potential barriers of up to 200 meV at the active p-n junction and at grain boundaries between CGSe crystallites, as inferred from KPFM cross-sectional studies.

The formation of an interfacial $MoSe_2$ layer at the rear contact under typical processing conditions during the growth of CGSe films has been monitored and compared to results reported in the literature. Several factors have been identified to affect the formation of this layered compound, including the Na-content of the glass substrates, the elemental content in the gas phase during processing and the substrate conditioning. Microstructural analyses have revealed a singular rearrangement of the van der Waals planes of this compound, which results in a smooth transition from type I to type II orientation. This characteristic change in the orientation of the van der Waals planes takes place under the concurrence of sufficient provision of Se and Ga species.

The general conclusions drawn from the structural analysis of CVD-CGSe films and related devices have been applied to the optimisation of the deposition process. Two approaches have been presented in this Chapter, which have demonstrated to overcome some of the difficulties related to the single stage processing of CGSe addressed before. These approaches, based on the implementation of sequential deposition recipes and on the use of Cu-precursors, take advantage of the flexibility of the open-tube CVD system, which provides unique features compared to other deposition processes based on chemical transport.

The two-stage process combines the advantages of a nearly stoichiometric first-stage growth, resulting in optimal film microstructure, and of the Ga- and Se- enrichment second stage, which finely tunes the electronic properties of the films to be used as absorbers. Structural studies have experimentally demonstrated this point. The two-stage process prevents the appearance of copper selenide segregations in the CGSe layers and additionally improves the electronics of the absorber layers, as observed from cross-sectional studies on complete solar cells by means of KPFM. In this respect, a

sputter cleaning process, designed for the treatment of samples exposed to air, has been tested and discussed, in order to provide reliable work function values from the KPFM measurements.

Processing on Cu-precursors has been analogously analysed, resulting in similar potential advantages as the sequential deposition process, with the possibility of downscaling the deposition time, due to an enhanced growth rate compared to standard processing on Mo-coated glass substrates. Two methods have been tested, including full two-stage processing and annealing treatments under Ga_xCl_y and H_2Se atmosphere, leading in both cases to the growth of closed films of single phase CGSe.

A third approach has been mentioned as a potential candidate for high-PV performance of CGSe-based thin-film solar cells, based on the lift-off process of the absorber, taking advantage of the role of the $MoSe_2$ interfacial layer in the mediation of the rear contact. This option will be analysed Chapter 5.